

OPTMIZATION OF AN INTAKE MANIFOLD FOR AN INTERNAL COMBUSTION

ENGINE

Burke M. Davis

I hereby release this thesis to the public. I understand that this thesis will be made available from the OhioLINK ETD Center and the University Library Circulation Desk for public access. I authorize the University or other individuals to make copies of this thesis as needed for scholarly research.

Burke M. Davis

Signature:

[Handwritten Signature]

Submitted in Partial Fulfillment of the Requirements

[Handwritten Date]
Date

for the Degree of

Aggregator:

Master's

in the

[Handwritten Signature]

[Handwritten Date]
Date

Mechanical Engineering

Program

[Handwritten Signature]
[Handwritten Signature]

[Handwritten Date]
Date

[Handwritten Signature]
[Handwritten Signature]

[Handwritten Date]
Date

YOUNGSTOWN STATE UNIVERSITY

May, 2006

[Handwritten Signature]
[Handwritten Signature]

[Handwritten Date]
Date

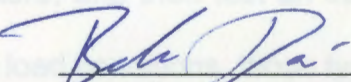
Peter J. Kasvisky, Dean of Graduate Studies and Research

Optimization of an Intake Manifold for an Internal Combustion Engine

Burke M. Davis

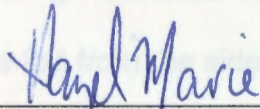
I hereby release this thesis to the public. I understand that this thesis will be made available from the OhioLINK ETD Center and the Maag Library Circulation Desk for public access. I authorize the University or other individuals to make copies of this thesis as needed for scholarly research.

Signature:


Burke Davis, Student

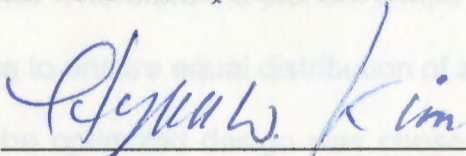
5/8/2006
Date

Approvals:



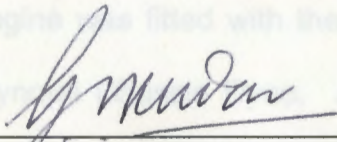
Dr. Hazel Marie, Thesis Advisor

05-08-2006
Date



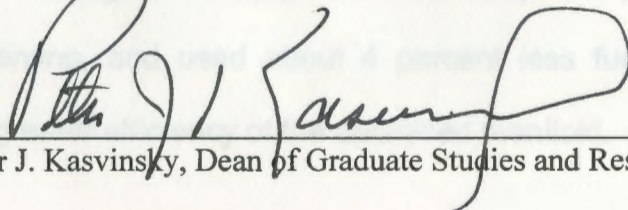
Dr. Shawn Kim, Committee Member

5-9-06
Date



Dr. Ganesh Kudav, Committee Member

5/8/2006
Date



Peter J. Kasvinsky, Dean of Graduate Studies and Research

5/9/06
Date

ABSTRACT

A methodology for the optimization of an intake manifold for an internal combustion engine was proposed and tested in this research. The test bed was a 1.8L turbocharged four-cylinder Honda engine. The goal was to design, manufacture, and then test an intake manifold optimized for high rpm operation and high load conditions, those typically seen in drag racing.

The runner's size and length and plenum size were first tuned for the operating rpms using Helmholtz equations. Due to the layout of the engine, the intake manifold is fed from the side which leads to mass flow rate inconsistencies in the cylinders. Therefore the plenum shape was optimized using computational fluid dynamics to ensure equal distribution of air to all cylinders.

After the optimized design was chosen, it was manufactured from sheet metal. The engine was fitted with the stock and optimized manifolds and dyno tested on a Dynojet Chassis Dyno. At similar boost pressures, the optimized manifold made an average of 1.5 hp/psi above 5000 rpm, required approximately 3 degrees less timing, and used about 4 percent less fuel, all of which are testament to the greater efficiency of the optimized manifold.

TABLE OF CONTENTS

ACKNOWLEDGEMENTS:

PAGE

ABSTRACT

ii

Dr. Hazel Marie

iv

Dr. Shawn Kim

v

Dr. Ganesh Kudav

vii

YSU Machine Shop

x

Akron Horsepower

1

Jenna Cramer

10

Eric Latimer

14

Sean Lindsey

34

James Gasper

56

TABLE OF CONTENTS

	PAGE
ABSTRACT	iii
ACKNOWLEDGEMENTS	iv
LIST OF FIGURES	vi
LIST OF TABLES	viii
NOMENCLATURE	ix
CHAPTER I – INTRODUCTION	1
CHAPTER II – SCOPE OF WORK	10
CHAPTER III – ANALYTICAL AND NUMERICAL OPTIMIZATION	14
CHAPTER IV – RESULTS	34
CHAPTER V – CONCLUSIONS	56
3.5 Meshed Gambit Model Showing Fluid Volumes	30
3.9 Fluent Model for Boundary Condition 0 where only Runner 1 is open	31
3.10 Plenum Dimensions for Optimized Manifold	33
3.11 Mass Flow Rate with Respect to Cam Timing	33
3.12 Mass Flow Rate as Compared to Runner 1 with Respect to Cam Timing	34
4.1 Stock Variable Geometry Acure Integr's GSR Intake Manifold	35
4.2 Optimized Intake Manifold On the Car	35
4.3 Engine Control Schematic	36
4.4 Parameters that are Logged	37
4.5 Fuel Table in Tabular Format	38
4.6 Fuel Table in Graphical mode	38
4.7 Fuel Table in Injector Duty Cycle	39

LIST OF FIGURES

Figure Number	Figure Title	Page Number
1.1	Intake Manifold Placement.....	1
1.2	Illustration Showing Injector Placement.....	3
2.1	VTEC Cams.....	12
3.1	Pressure Distribution with Runner 1 Port Open.....	23
3.2	Valve Position With Respect to Degrees of Engine Rotation.....	24
3.3(a)	Mass Flow Rate with Respect to Engine Timing.....	26
3.3(b)	Mass Flow Rate with Respect to Cam Timing.....	26
3.4	Mass Flow rate as Compared to Runner 1 with Respect to Cam Timing...	27
3.5(a)	Outlet Velocities with respect to Engine Timing.....	28
3.5(b)	Velocities with Respect to Cam Timing	28
3.6	Velocities as Compared to Runner 1.....	29
3.7	Solidworks Solid Model of Optimized Model.....	30
3.8	Meshed Gambit Model Showing Fluid Volumes.....	30
3.9	Fluent Model for Boundary Condition 0 where only Runner 1 is open.....	31
3.10	Plenum Dimensions for Optimized Manifold.....	33
3.11	Mass Flow Rate with Respect to Cam Timing.....	33
3.12	Mass Flow Rate as Compared to Runner 1 with Respect to Cam Timing..	34
4.1	Stock Variable Geometry Acura Integra GSR Intake Manifold.....	35
4.2	Optimized Intake Manifold On the Car.....	35
4.3	Engine Control Schematic.....	36
4.4	Parameters that are Logged.....	37
4.5	Fuel Table in Tabular Format.....	38
4.6	Fuel Table in Graphical mode.....	38
4.7	Fuel Table in Injector Duty Cycle.....	39

4.8	Ignition Table in Tabular Format.....	39
4.9	Ignition Table in Graphical Mode.....	40
4.10	Head Flange That Fits All VTEC Heads.....	41
4.11	Fluted Venturi's on Runner Entrance.....	42
4.12	Runner Taper Welded to Head Flange.....	42
4.13	The Remote Mounted Idle Air Control Valve.....	43
4.14	Vacuum Ports and Air Intake Temperature Sensor	44
4.15	Power Output for Stock Manifold vs. Boost Pressure.....	45
4.16	Power Output for Optimized Manifold vs. Boost Pressure.....	48
4.17	Power Output for Stock and Optimized Manifolds With Boost Pressure....	51
4.18	Ignition Advance vs RPM for 7.8 psi.....	52
4.19	Injector Duty vs RPM for 7.8 psi.....	53
4.20	Fuel Injector Duty Cycle for 11.5 psi.....	53
4.21	Comparison of Power Output Per Amount of Fuel Consumed.....	54
4.22	Power Output Per Psi of Boost vs Engine Speed.....	55
5.1	Final Dimensions of Plenum Shape.....	59

LIST OF TABLES

Table Number	Table Title	Page Number
3.1	Valve Position With Respect to Degrees of Engine Rotation	24
3.2	Results of Flow Rate Differences for the Nine Manifold Configurations.....	33
4.1	Ignition Advance for Low Cam Operation at Operating Boost Pressures.....	46
4.2	Ignition Advance for High Cam Operation at Operating Boost Pressure.....	46
4.3	Injector Duty Cycle for Low Cam Operation at Operating Boost Pressures..	47
4.4	Injector Duty Cycle for High Cam Operation at Operating Boost Pressures..	47
4.5	Ignition Advance for Low Cam Operation at Operating Boost Pressures.....	49
4.6	Ignition Advance for High Cam Operation at Operating Boost Pressures.....	49
4.7	Injector Duty Cycle for Low Cam Operation at Operating Boost Pressures...	49
4.8	Injector Duty Cycle for High Cam Operation at Operating Boost Pressures..	50

A_2 = cross-sectional area of intake tract in head (in²)

L_2 = length of intake tract in head (in)

r = compression ratio of engine

h = distance from the base of the plenum to the top of the runner inlet (in)

b = horizontal length of plenum top (in)

y = vertical length of plenum side (in)

NOMENCLATURE

n = resonant frequency (Hz)

c = velocity of sound in air (m/s)

A = cross-sectional area of tuned pipe (m^2)

L = length of tuned pipe (m)

V = resonating volume (m^3)

N = Tuned Engine Speed (RPM)

A_1 = cross-sectional area of runner (in^2)

L_1 = length of runner (in)

A_2 = cross-sectional area of intake tract in head (in^2)

L_2 = length of intake tract in head (in)

r = compression ratio of engine

h = distance from the base of the plenum to the top of the runner inlet (in)

b = horizontal length of plenum top (in)

y = vertical length of plenum side (in)

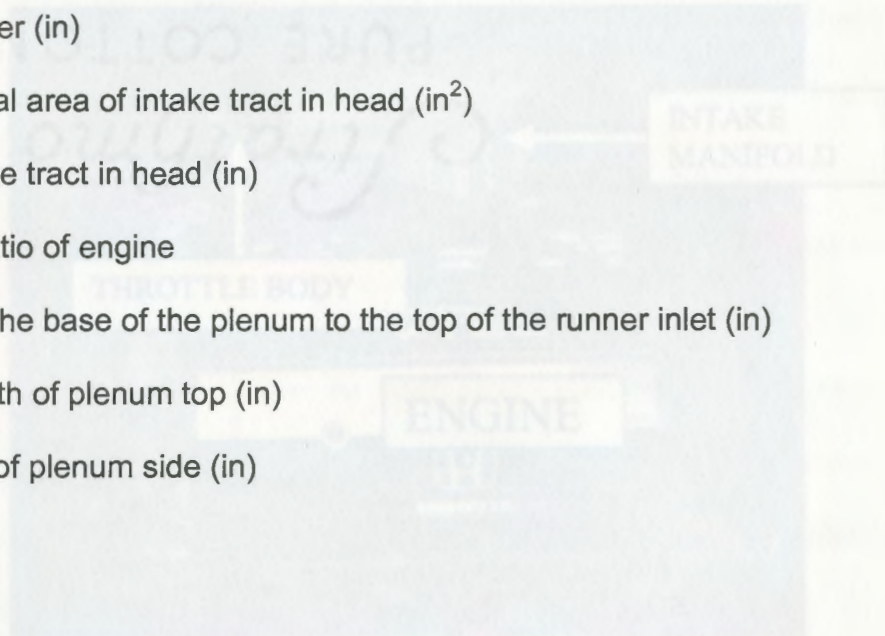


Figure 1.7: Intake Manifold Placement

Intake manifolds have always been a part of internal combustion engines. However, they have changed a great deal from the days of the carburetor. With

CHAPTER I

INTRODUCTION

1.1 Background

Intake manifolds play a critical role in an internal combustion engine. Not only do they distribute the air to the engine, but they also have a profound effect on the characteristics of the engine. The intake manifold resides between the throttle body and the cylinder head, Figure 1.1.

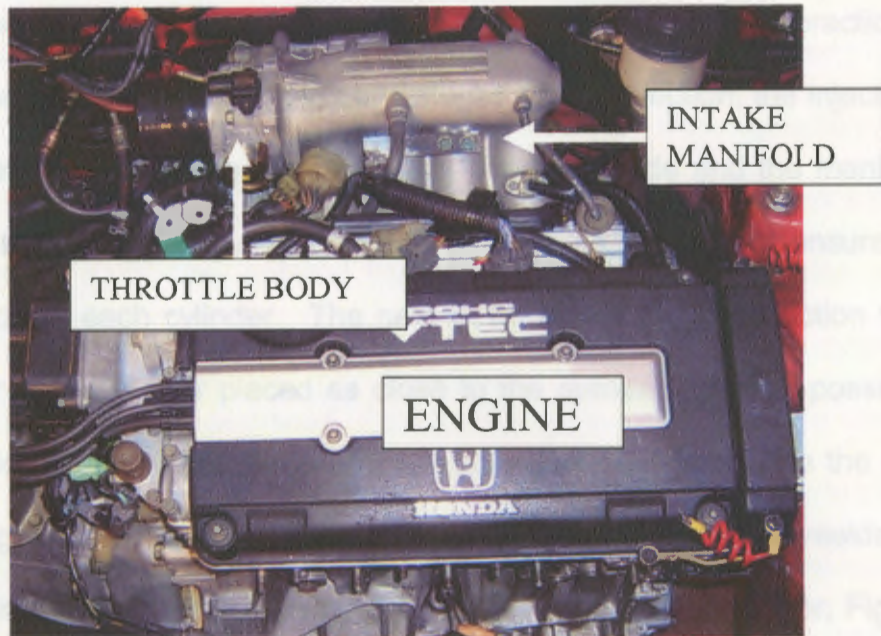


Figure 1.1: Intake Manifold Placement

Intake manifolds have always been a part of internal combustion engines. However, they have changed a great deal from the days of the carburetor. With

a carburetor, the design of the manifold is limited due to the fact that the carburetor must sit on top of the intake manifold. This is so that the air rushing past the carburetor can pull the fuel out and into the engine. Optimally all of the runners would be the same length to aid in equal distribution of air, but with all runners having to merge at the same point, the lengths must be different. This could be partly overcome by using multiple carburetors. The ideal carburetor setup is one carburetor for each runner and is often the case in motorcycle engines or high performance carbureted engines.

While carburetors are still used in some of the most powerful engines in racing today, they simply cannot meet today's strict emissions requirements, because of the inability to accurately moderate the fuel delivery over all loading and engine speed (rpm) conditions. Therefore fuel injection is used in practically every production engine today. In the early stages of fuel injection, the injectors, usually two, were placed where the carburetor used to reside and the manifold then delivered the air-fuel mixture to the cylinders. This still did not ensure an equal distribution to each cylinder. The next development in fuel injection was one injector for each cylinder placed as close to the cylinder head as possible. This configuration is often referred to as multi-point fuel injection and is the one used on the engine chronicled in this research. The individual injectors reside on the intake manifold at about a 45 degree angle at the exit of the runner, Figure 1.2.

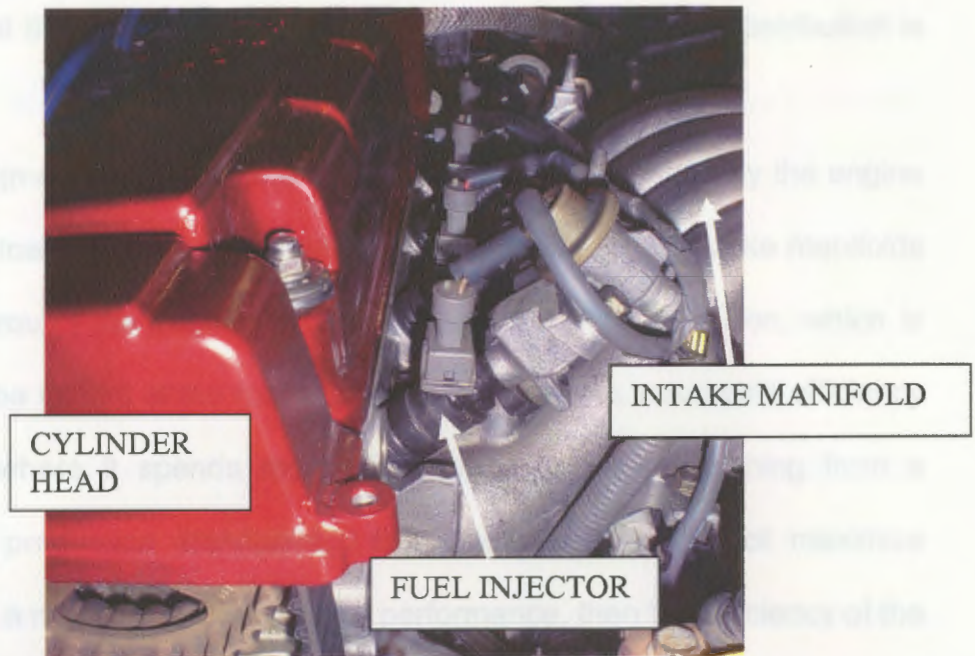


Figure 1.2: Illustration Showing Injector Placement

The intake manifold is for a four cylinder configuration with the throttle body next to the number 4 cylinder on the far end of the plenum, making it an asymmetrical design, Figure 1.1. Because of this, the length from the inlet to the exit for each port is different. Therefore, it seems intuitive that pressure losses will be different for each one, making the mass flow rates different for each cylinder. This means that different amounts of oxygen enter each cylinder. However, the amount of fuel delivered to each cylinder is same because almost every engine management system delivers the same pulse width and latency, how fast the injector opens, to each fuel injector. As a result, the air/fuel ratio is different in each cylinder, meaning each cylinder's combustion properties, temperature, and pressure will be different, making it harder to control the emissions and properties of the engine. If the cylinder's temperature becomes too high, it can lead to predetonation also known as knocking or pinging, which

will severely limit the life of the engine. Therefore the most equal distribution is desired.

The design of an intake manifold greatly affects how efficiently the engine runs for certain loading and rpm conditions. For the most part, intake manifolds are designed around the engines most common operating condition, which is somewhere in the middle of the rpm range. This raises the volumetric efficiency of the engine where it spends most of its operation; a good thing from a consumer and production standpoint. But these designs do not maximize performance. If a manifold is designed for performance, then the efficiency of the engine is lacking at low-to-mid-range engine speeds. Some car manufactures have found a partial solution for optimization between low and high-end performance using a variable runner size and variable plenum size. This is usually employed with a vacuum operated butterfly valve that opens the high rpm runners at a predetermined rpm or a butterfly valve that opens the secondary plenum chamber. An example of the variable plenum is VRIS (Variable Resonance Intake System) which is employed in the 93-97 Ford Probe GT. An example of the secondary runner system is the intake manifold for the Honda Prelude and the Acura Integra GSR, which will be employed in this research.

1.2 Intake Manifold Literature Review

The design process outlined in this paper is closely related to the design process done in the industry, except some of the variables have been taken out because much of the preliminary design has already been done. This research

is an optimization of an intake manifold for use in turbocharged applications; although similar gains could be seen in naturally aspirated applications as well. For the optimization process, the size and length of the primary runners and the volume of the plenum were found using the processes discussed subsequently, while the plenum shape and runner entrance were optimized with the aid of computational fluid dynamics (CFD), presented in Chapter 3.

Vorum, 1980, presented a study on the intake and exhaust designs for four-stroke engines. He used Helmholtz defined pressure excursions to maximum ram charging in intakes and scavenging for exhausts. He described both a one-and two-degree of freedom system. The research showed that using the volume of the piston along with the size, volume, and length of the runner was negligible to the overall effect of the Helmholtz design. A shorter pipe, resulting from a higher design speed would greatly reduce the ripples in pressure variation in the intake pipe, leaving a broad Helmholtz defined curve. He provides a good explanation of the Helmholtz design:

[The pressure depression during the opened period is similar to the events in a venture. As velocity goes up, the static pressure goes down. As it exits, it has some velocity but is near atmospheric pressure. The vacuum it pulls will help do pump work for the next intake stroke. By timing the vacuum peak and matching it to an optimum velocity, maximum work is done by the air in the pipe.]

He also stated that abrupt corners and bends are not optimal because of flow losses which are as discussed in depth by Talloi et al, 1993, but they have no change in the tuning rpm. Another rule of thumb Vorum discussed is that an area change from 2-1 or more entering or leaving a plenum is desirable. The optimum radius of curvature for good flow characteristics of the entrance should be between 20 and 25% of the radius of the runner.

Talloi et al, 1993, goes more in depth concerning flow loss where the purpose of his research was to examine the geometry induced flow losses in intake manifold designs. Based on their assumptions, four intake manifolds were designed and compared numerically and experimentally. The findings showed that the primary runner entrance accounted for over half of the total system loss. The authors used two manifolds, one with a bell shaped inlet and one with a squared inlet. Both were analyzed with a constant and a variable cross-sectional plenum.

The experimental setup included the engine placed on an engine dynamometer where the temperature, pressure, injector pulse and latency, air/fuel mixture, and emissions were measured. The volumetric efficiency for the operating rpm range was then calculated and plotted for all four of the scenarios. The research found that the bell mouth design was best entrance design, and the no plenum was better than a plenum. The intake pressure was also recorded using a fast acting pressure transducer and plotted as a function of the crank angle. Further, the pressure was analyzed in the frequency domain. It showed

the primary frequency to correspond with the standing wave frequency at 4000 rpm as was expected.

The equations used by Talloi et al 1994, are the beginnings of the Helmholtz equations which were used by Brands, 1979, in his study of a tuned intake system. In his research a tuned induction system using a Helmholtz resonator, was applied to an in-line 6 cylinder diesel engine. The system was designed to add an additional increase in torque at the peak torque engine speed. The tuned intake improved volumetric efficiency at that point by 12 percent, improved the air distribution to the cylinders, and caused faster turbocharger response. At the time of his work, however the experimental and testing procedures were limited compared to today's standards. The engine was tested on a dynamometer, the amount of fuel consumed was recorded, and the cylinder pressure was used to determine the volumetric efficiency. This is similar to the way that the effectiveness of the designed intake manifold of this research was done.

Ganesan et al, 2003 have done CFD analysis on the flow patterns of air inside an intake manifold. The work was more of a validation on an existing model, with no real optimization presented. Ganesan et al, presented their CFD procedure and results of the air flow through an air intake system of a three cylinder engine. The analysis of the air flow included from the throttle plate through the plenum to the intake manifold to the intake valve. The solid model was created in Solidworks and then transported to Gambit where it was meshed using a Tet-hybrid scheme and the boundary conditions were added. It was then

exported to Fluent where the numerical values for the boundary conditions and rest of the model data was entered.

Their objective was to analyze the flow at idle, part throttle and wide open throttle and to validate the prediction by comparing to experimental data. The model was analyzed using the turbulent k-e model with a constant density. The boundary condition at the inlet was a simple pressure-inlet condition where the pressure is known, but not the mass flow rate or velocity. For the outlet ports, pressure outlet boundary conditions were used.

The model was analyzed at various outlet pressures for the various cylinders at each of the stated conditions. Because it is a three cylinder engine, only one valve is open at a time, therefore only steady state analysis was done with each valve opened at maximum lift for the different outlet pressures. The mass flow rates were found and plotted for each cylinder as a function of the outlet pressures. Plots of the velocity vectors were also studied with respect to abnormal eddy currents, which did exist. The model data corresponded very well with experimental data with the percent difference being within 5%. Ganesan et al concluded that CFD analysis is a very useful tool in developing intake manifold and can be employed in the optimization of an intake manifold design.

Safari, 2003, also used Fluent to analyze an intake manifold for a 1.6 liter engine developed by Volkswagen. Steady and unsteady analysis was done. The boundary conditions were not explicitly given in the paper, but it can be assumed from the wording and figures that they used a constant pressure inlet and a varying pressure outlet in transient study. Again, model validation

optimization was not the focus. Safari did give suggestions for optimization, such as smoothing some hard edges, changing the placement of the throttle body, and stating that the plenum is not optimal.

CHAPTER 4

SCOPE OF WORK

The optimization of the design of the intake manifold for high engine speeds with increased pressure and mass flow rates was accomplished utilizing both numerical analytical modeling and experimental data acquisition. The numerical analysis includes the geometry being defined by Helmholtz resonance. After the dimensions were chosen, Computational Fluid Dynamics (CFD) was performed using the commercial package Fluent to optimize the geometry of the runners and plenum to ensure equal distribution to all cylinders. The manifold was designed based on combining the results of the numerical and fluid analysis. The effectiveness is evaluated by comparing the torque curves, fuel consumption, and timing of stock and optimized manifolds.

CFD was first performed using a simple 2-D model representative of the actual model to ensure the correctness of boundary conditions and CFD processes and monitors. Steady-state and transient models are analyzed with the parts being opened and closed according to the cam lift and duration.

The optimized manifold's effectiveness was seen by the change in power output of the engine. The torque for the stock and optimized manifold was measured on a dynamometer. The efficiencies of the manifolds were determined

by analyzing the torque, fuel consumption, and timing at each load and rpm condition. The fuel consumption was measured by analyzing the duty cycle of the fuel injectors.

CHAPTER II

SCOPE OF WORK

The optimization of the design of the intake manifold for high engine speeds with increased pressure and mass flow rates was accomplished utilizing both numerical/ analytical modeling and experimental data acquisition. The numerical analysis includes the geometry being defined by Helmholtz resonance. After the dimensions were chosen, Computation Fluid Dynamics (CFD) was performed using the commercial package Fluent to optimize the geometry of the runners and plenum to ensure equal distribution to all cylinders. The manifold was designed based on combining the results of the numerical and fluid analysis. The effectiveness is evaluated by comparing the torque curves, fuel consumption, and timing of stock and optimized manifolds.

CFD was first performed using a simple 2-D model representative of the actual model to ensure the correctness of boundary conditions and CFD processes and monitors. Steady-state and transient models are analyzed with the ports being opened and closed according to the cam lift and duration.

The optimized manifold's effectiveness was seen by the change in power output of the engine. The torque for the stock and optimized manifold was measured on a dynamometer. The efficiencies of the manifolds were determined

by analyzing the torque, fuel consumption, and timing at each load and rpm condition. The fuel consumption was measured by analyzing the duty cycle of the fuel injectors.

While the stock 1.8L Acura Integra GSR manifold performs well because of the secondary intake runners, it was still a compromise between low and high rpm performance. Also, this intake manifold was not designed for the turbocharged engine, therefore it was designed using mass flow rates, pressures, and velocities that no longer existed. Further, the engine that was used as the test bed for this intake manifold design did not come from the factory. The engine block is b18a1, 1.8L from an Acura Integra LS with a displacement of 1834cc with 130hp from the factory, while the head is from a b18c1 from an Acura Integra GSR with a displacement of 1797cc with 170hp. They both however share the same basic block architecture such that switching heads was a relatively easy process. The extra 40hp from b18c1 comes from the head, which employs the VTEC valve train technology which stands for variable valve timing and electronic lift control. VTEC essentially gives the engine two cam profiles on one cam; one for low-to mid-range conditions and one maximized for high rpm performance. A picture of a VTEC cam is shown in Figure 2.1. Note that the large lobe in the middle, which is for the high rpm operating conditions, is often referred to as the VTEC lobe. When on the high rpm lobe, it is often called engaging VTEC or being "in VTEC". By placing the b18c1 VTEC head on the b18a1 rotating assembly, one gets the best performance from a b series engine; larger displacement from the b18a1 and the

better flowing head from the b18c1. This engine configuration is often referred to as an LS-VTEC because of the LS bottom end from the Acura Integra LS and the VTEC head from the GSR.

This LS-VTEC engine was coupled to a short ratio GSR transmission for maximum acceleration and resides in a 1994 Honda Civic Hatchback. The hatchback shares the same chassis as the Integra, but is much lighter than its Acura counterpart. The engine was also fitted with an internally wastegated Garrett T3/T04b turbocharger. The turbocharger compresses the outside air and when doing so generates heat, therefore an air-to-air intercooler was used to lower the engine's air temperature. A 3 inch down pipe and exhaust was used to minimize back pressure on the turbine, thereby raising its efficiency.

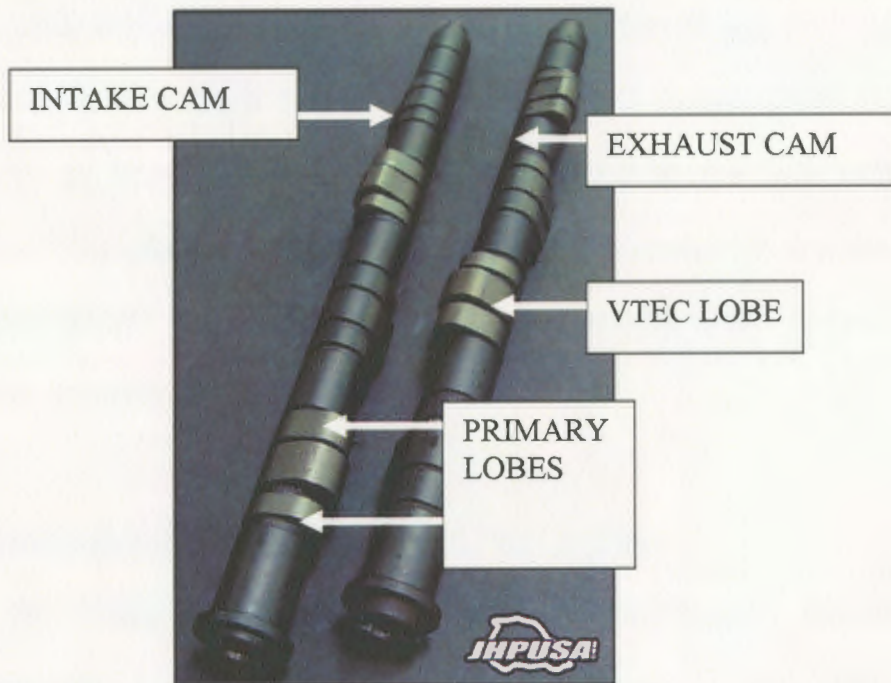


Figure 2.1 – VTEC Cams

The engine is controlled by a standalone engine management system which uses a modified stock computer that allows the engine to run the larger injectors and has the ability to record and change any of the engines parameters. This is very beneficial because of the ease of monitoring the engine's operating conditions such as manifold pressure, air-fuel ratio, air temperature, rpm, and more.

The development of the optimized intake manifold was done in two stages. First the runner length, size, and plenum volume were designed to a specific engine speed using Helmholtz frequency tuning. After the plenum size was chosen, its shape was analyzed using CFD to minimize flow variations and losses and optimize equal distribution to all cylinders. It was analyzed in both a steady-state and in an unsteady model. A 2-D model was first created to test the boundary conditions and process for the 3-D model. Once perfected, the methodology from the 2-D model was adapted to the 3-D with immediate success. The steady analysis proved to not be useful for analysis because it produced results opposite of the real world results which coincided with the unsteady analysis.

3.1 Optimization of Runner Length and Plenum Size

The runner length and plenum size were optimized to the tuned RPM of approximately 6000 RPM using Helmholtz tuning. The basic Helmholtz resonator consists of a chamber with a pipe projecting from it. The chamber

being the plenum and the pipe being the intake runner extending to the back of the intake valves, this runner then becomes the tuned intake tract.

3.1.2 Helmholtz Theory

CHAPTER III

ANALYTICAL AND NUMERICAL OPTIMIZATION

The development of the optimized intake manifold was done in two stages. First the runner length, size, and plenum volume were designed to a specific engine speed using Helmholtz frequency tuning. After the plenum size was chosen, its shape was analyzed using CFD to minimize flow variations and losses and optimize equal distribution to all cylinders. It was analyzed in both a steady-state and in an unsteady model. A 2-D model was first created to test the boundary conditions and process for the 3-D model. Once perfected, the methodology from the 2-D model was adapted to the 3-D with immediate success. The steady analysis proved to not be useful for analysis because it produced results opposite of the real world results which coincided with the unsteady analysis.

3.1 Optimization of Runner Length and Plenum Size

The runner length and plenum size were optimized to the tuned RPM of approximately 6000 RPM using Helmholtz tuning. The basic Helmholtz resonator consists of a chamber with a pipe projecting from it. The chamber

$V =$ resonating volume (m^3)

being the plenum and the pipe being the intake runner extending to the back of the intake valves, this runner then becomes the tuned intake tract.

3.1.2 Helmholtz Theory

The Helmholtz resonator is analogous to a mechanical spring-mass model where the tuned frequency is proportional to the gas velocity and system geometry, Brands, 1979. Every time the intake valve opens, a disturbance is created in the intake tract and a negative pressure-wave pulse is sent back up the runner and into the plenum. Once the wave reaches the end of the pipe, a positive pulse is reflected back towards the intake valve. If timed correctly these waves bombard the cylinder with surges of compressed air towards the end of the piston's stroke where the vacuum created by the downward movement of the piston is least, Heisler 1996. This results in cramming more air into the cylinder before the inlet valve closes. The downside is that this tuning can only be done for one rpm. The Helmholtz equation is shown in Equation 3.1

$$n = \frac{c}{2\pi} \sqrt{\frac{A}{LV}} \quad 3.1$$

where

n = resonant frequency (Hz)

c = velocity of sound in air (m/s)

A = cross-sectional area of tuned pipe (m^2)

L = length of tuned pipe (m)

V = resonating volume (m^3)

The Helmholtz equation can be written differently. For this research it was written in the form by Vorum, 1980,

$$N = 77c \sqrt{\frac{\frac{A_1}{L_1} + \frac{A_2}{L_2} r - 1}{V r + 1}} \quad 3.2$$

where

N = Tuned Engine Speed (RPM)

c = velocity of sound in air (ft/s)

A_1 = cross-sectional area of runner (in²)

L_1 = length of runner (in)

A_2 = cross-sectional area of intake tract in head (in²)

L_2 = length of intake tract in head (in)

V = plenum volume (in³)

r = compression ratio of engine

Equation 3.2 accounts for the changing diameters of the runner and intake tract, which is why this method was chosen. Many variations do not account for the changing diameters or assume that the runner diameter is the same as the intake tract. In this research, a larger diameter was used to minimize flow losses at high mass flow rates, specifically under high boost conditions, therefore the separate diameters had to be accounted for.

Another verification of Helmholtz tuning based solely on the primary pipe length, diameter, and plenum volume is demonstrated Winterbone and Pearson, 1999, and stated as below

$$\tan\left(\frac{\omega l_p}{a}\right) = \frac{a F_p}{\omega V_c} \quad 3.3$$

where

ω = Tuned Frequency (rad/s)

l_p = Length of Primary Runner (in)

a = Speed of Sound in Air (in/s)

F_p = Primary Runner Diameter (in²)

V_c = Plenum Volume (in³)

This equation completely ignores the intake tract in the head and the compression ratio, but it does yield results close to Equation 3.2.

3.1.3 Numerical Results

Base line dimensions were chosen for the plenum shape based on physical constraints in the engine bay. The final shape was based on CFD analysis and had a total volume, V of 248 in³. An estimation of the area of the inlet tract in the head, A_2 , was taken as the cross-sectional area of the inlet port which was 2.3 in² even though the area does change as it splits to go to the separate valves. The intake tract length, L_2 , was measured to be approximately 3 inches from the opening of the inlet to the base of the valve. The compression ratio, r , of the engine is known to be 10:1. The estimation of the operating conditions, 120 °F, yielded the speed of sound in air, c , to be 1125 ft/s. The diameter of the runners was chosen to be 2.25 in ($A_1 = 3.98$ in²) because of availability of the stock, the ease of manufacturing, and it offered a sufficient

transition to the intake tract. The design tuned engine speed, N , of 6000 rpm was chosen so that the manifold would make more power in the higher powerband where the engine operates under racing conditions. When computed in Equation 3.2, a runner length of 7 inches was chosen. These same values were also input into Equation 3.3 and yielded a design speed of 6175 rpm, which is quite close to the overall design speed of 6000 rpm.

3.2 Governing Equations of Fluent

The core of the Fluent solver is its flow module. This model solves the x-, y- and z-momentum and continuity equations. From these equations it derives a solution for the velocity fields and solves the pressure field by solving the pressure correction equation. These governing equations represent the conservation laws of physics for flow, with the continuity equation being the conservation of mass and the momentum equations, being Newton's second law; the conservations of momentum, respectively.

The conservation of mass requires that the time rate of change of mass in the control volume is balanced by the net mass flow out of the control volume.

This can be expressed as

$$\frac{\partial \rho}{\partial t} + \nabla \cdot \rho \vec{V} = 0 \quad 3.4$$

where

$$\frac{\partial \rho}{\partial t} \equiv \text{rate of change of the density inside control volume boundaries}$$

$$\nabla \cdot \rho \vec{V} \equiv \text{net mass flow across the control volume boundaries}$$

$\nabla \equiv$ vector operator in rectangular coordinates, $\hat{i} \frac{\partial}{\partial x} + \hat{j} \frac{\partial}{\partial y} + \hat{k} \frac{\partial}{\partial z}$

Newton's second law states that the time rate of change of the momentum of a fluid element is equal to the sum of the forces on the element. There are two types of forces on a fluid element; surface forces which are pressure forces and viscous forces and body forces, such as gravity, centrifugal and electrometric forces, etc. The x-component of the momentum equations is solved by setting the rate of change of x-momentum of the fluid particle equal to the total force in the x-direction on the element, plus the increase of x-momentum due to the sources. The y- and z- component equations are defined similarly. With the surface forces expanded and the body forces kept as a single body force source term, the momentum equations are expressed as

$$\frac{\partial(\rho u)}{\partial t} + \nabla \cdot \rho \vec{V} u = dF_{Bx} + \frac{\partial \sigma_{xx}}{\partial x} + \frac{\partial \tau_{yx}}{\partial y} + \frac{\partial \tau_{zx}}{\partial z} + S_{Mx} \quad 3.5(a)$$

$$\frac{\partial(\rho v)}{\partial t} + \nabla \cdot \rho \vec{V} v = dF_{By} + \frac{\partial \tau_{xy}}{\partial x} + \frac{\partial \sigma_{yy}}{\partial y} + \frac{\partial \tau_{zy}}{\partial z} + S_{My} \quad 3.5(b)$$

$$\frac{\partial(\rho w)}{\partial t} + \nabla \cdot \rho \vec{V} w = dF_{Bz} + \frac{\partial \tau_{xz}}{\partial x} + \frac{\partial \tau_{yz}}{\partial y} + \frac{\partial \sigma_{zz}}{\partial z} + S_{Mz} \quad 3.5(c)$$

In these equations, \vec{V} is the fluid's total velocity vector; u , v , and w are the x-, y-, and z-direction fluid velocity components, respectively; σ_{ii} and τ_{ij} are the normal and shear viscous stress terms, respectively; dF_{Bi} is the differential body force component, and S_{Mi} is the momentum source term component.

For this research, the fluid is air considered to be a Newtonian fluid with constant density; therefore the viscous stresses are proportional of the

deformation rates. The viscous stress components, of which six are independent in the isotropic fluids, can be related to velocity gradients to produce the following relationships between viscous stress, velocity and pressure fields. In these equations, μ is the fluid dynamic viscosity and p is the thermodynamic pressure (related to the density and temperature of the fluid by the equation of state).

$$\tau_{xy} = \tau_{yx} = \mu \left(\frac{\partial v}{\partial x} + \frac{\partial u}{\partial y} \right) \quad 3.6(a)$$

$$\tau_{yz} = \tau_{zy} = \mu \left(\frac{\partial w}{\partial y} + \frac{\partial v}{\partial z} \right) \quad 3.6(b)$$

$$\tau_{zx} = \tau_{xz} = \mu \left(\frac{\partial u}{\partial z} + \frac{\partial w}{\partial x} \right) \quad 3.6(c)$$

$$\sigma_{xx} = -p - \frac{2}{3} \mu \nabla \cdot \vec{V} + 2\mu \frac{\partial u}{\partial x} \quad 3.6(d)$$

$$\sigma_{yy} = -p - \frac{2}{3} \mu \nabla \cdot \vec{V} + 2\mu \frac{\partial v}{\partial y} \quad 3.6(e)$$

$$\sigma_{zz} = -p - \frac{2}{3} \mu \nabla \cdot \vec{V} + 2\mu \frac{\partial w}{\partial z} \quad 3.6(f)$$

Substitution of the viscous stress terms in the momentum equations, neglecting body forces, yields the Navier-Stokes Equations, which are written as follows.

$$\frac{\partial(\rho u)}{\partial t} + \nabla \cdot \rho \vec{V} u = -\frac{\partial p}{\partial x} + \nabla \cdot (\mu \nabla u) + S_{Mx} \quad 3.7(a)$$

$$\frac{\partial(\rho v)}{\partial t} + \nabla \cdot \rho \vec{V} v = -\frac{\partial p}{\partial y} + \nabla \cdot (\mu \nabla v) + S_{My} \quad 3.7(b)$$

$$\frac{\partial(\rho w)}{\partial t} + \nabla \cdot \rho \vec{V} w = -\frac{\partial p}{\partial z} + \nabla \cdot (\mu \nabla w) + S_{Mz} \quad 3.7(c)$$

3.3 These three equations, with the continuity equation, form a set of coupled nonlinear partial differential equations for u , v , w , and p . Fluent uses the finite-volume approach, where the domain is divided into a number of cells known as control volumes. In this approach, the governing equations are numerically integrated over each divided control volume. There is no way to explicitly solve these equations, therefore an iterative process is employed at every time-step.

The solution of the three momentum equations yields the components of velocity, but pressure is left unknown because there is no governing PDE for it. Therefore Fluent utilizes the continuity equation to formulate an equation for pressure correction using an iterative scheme SIMPLEC (Semi-Implicit Method for Pressure-Linked Equations Consistent). The SIMPLEC procedure can be summarized as follows.

1. Guess, or use a previous iteration pressure field P^* .
2. Use P^* to obtain u^* , v^* , and w^* by solving the discretized momentum equations.
3. Check to see if the continuity equation is satisfied.
4. If not satisfied, determine P' , correction to P^* .
5. Use P' to correct the pressure field and to find corrections (u' , v' , and w') for the velocity fields. These corrections are the iteration residuals.
6. Solve the discretized equations for other flow variables, such as the enthalpy equation.
7. Go to step 2 and repeat the procedure until convergence is obtained by specifying maximum allowable values for the residuals.

3.3 Preliminary Fluent Analysis

Some preliminary work was done in Fluent using a simplified 2-D model of the manifold to verify the correct interface between Fluent and a journal file containing varying boundary conditions. This was done due to the fact that computational time required for a two dimensional study takes minutes while a comparable 3-D model takes hours to complete. This way any problems with conflicting boundary conditions and the setup for the transient study were identified quickly. The objective was to analyze the fluid flow of the intake manifolds in each runner, specifically the mass flow rate and velocity at the end of each runner as it entered the cylinder. Any shortcomings, such as abnormal turbulent flow, that would cause an additional pressure loss could also be seen from the CFD analysis.

In both the steady and unsteady analysis the throttle body is taken as a mass-flow-inlet where the direction, pressure, and mass flow rate are specified. This can be considered as a constant mass flow rate because the turbocharger flows a constant amount of air. Also, the small pressure variations due to the nature of a turbocharger are damped enough from the intercooler that these assumptions can be made. The outlets of the runners are taken as a pressure outlet with a pressure slightly less than that of the inlet to mimic the vacuum created by the downward movement of the piston. While this pressure does physically change, it is taken as constant since this simplifying assumption will still give accurate results of the variation of flow between the cylinders

All of the boundary conditions and analysis steps were the same for the two and three dimensional models. The throttle body was taken as a pressure inlet and each runner was either a pressure outlet with a pressure slightly lower than that of the inlet, or as a wall, Figure 3.1.

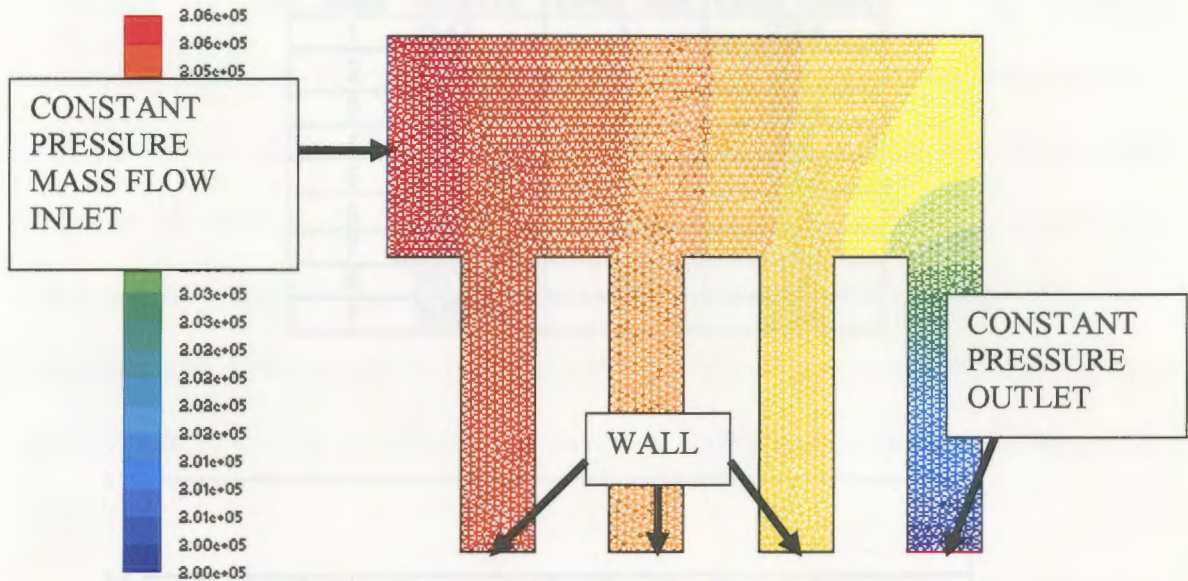


Figure 3.1 – Pressure Distribution with Runner 1 Port Open

The lower pressure at the outlet is caused from the rapid movement of the cylinder once the valve opens which creates a vacuum-type effect. When the valve is open the runner outlet is a pressure outlet which allows the fluid to pass through at the predetermined pressure. When the valve is closed the runner outlet becomes a wall and no fluid is able to be passed through it. The length each valve is open is determined by the duration of the intake cam which is 274 degrees. The cams are turned over one time for every two times the engine turns over, giving the cams a period of 720 degrees. Because of the length of the cam duration, there are times when one or two valves are open. The firing

order for this specific engine is 1-3-4-2. Table 3.1 and Figure 3.2 show the opening of the valves based on 720 degrees of engine rotation.

Table 3.1: Valve Position With Respect to Degrees of Engine Rotation

Stage	Degrees	Valves Open	Valves Closed
1	0-42	1	2,3,4
2	43-136	1,3	3,4
3	137-222	3	1,2,4
4	223-317	3,4	1,2
5	318-402	4	1,2,3
6	403-497	2,4	1,3
7	498-582	2	1,3,4
8	583-677	1,2	3,4
1	678-720	1	2,3,4

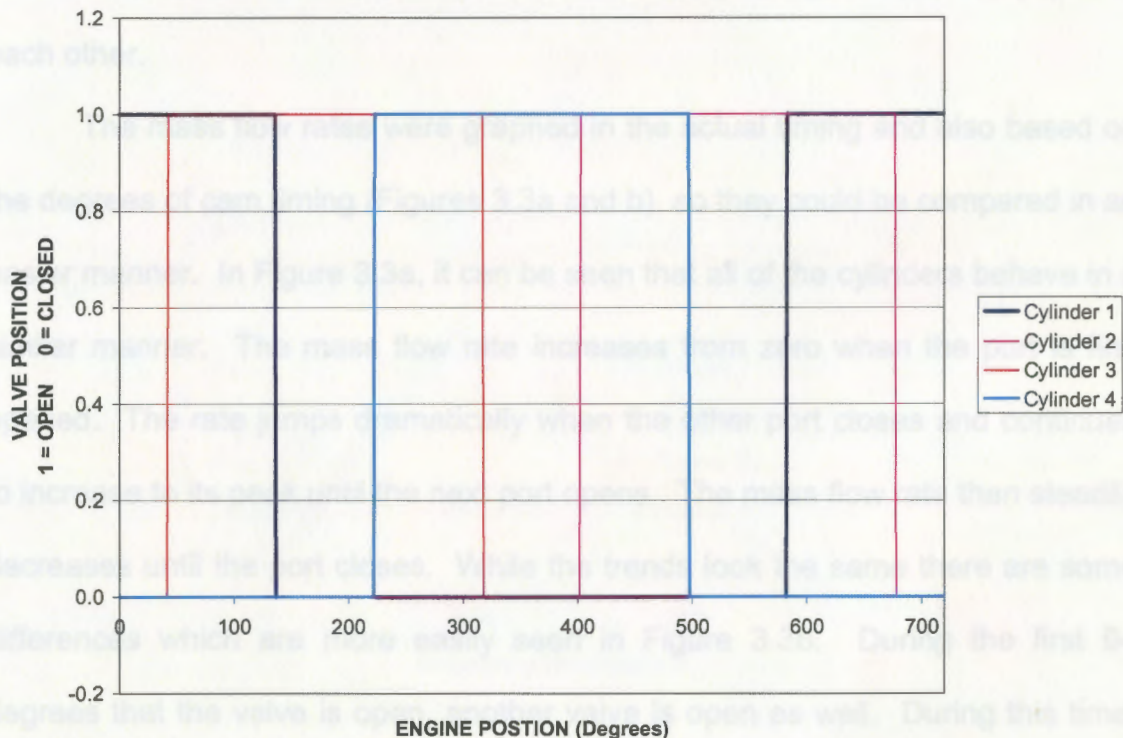
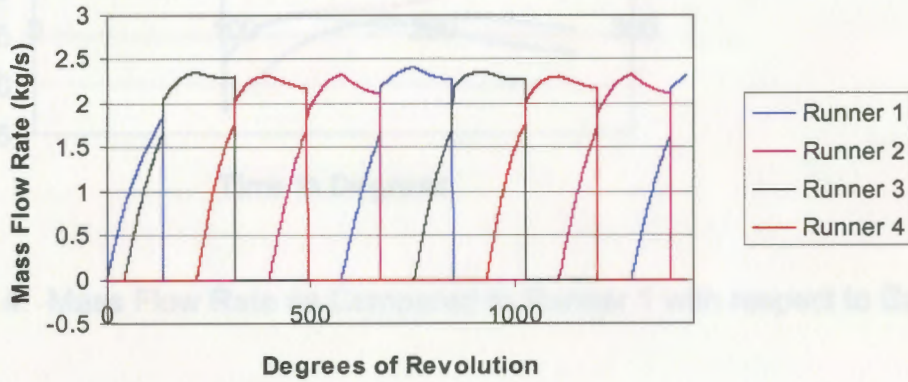


Figure 3.2: Valve Position With Respect to Degrees of Engine Rotation

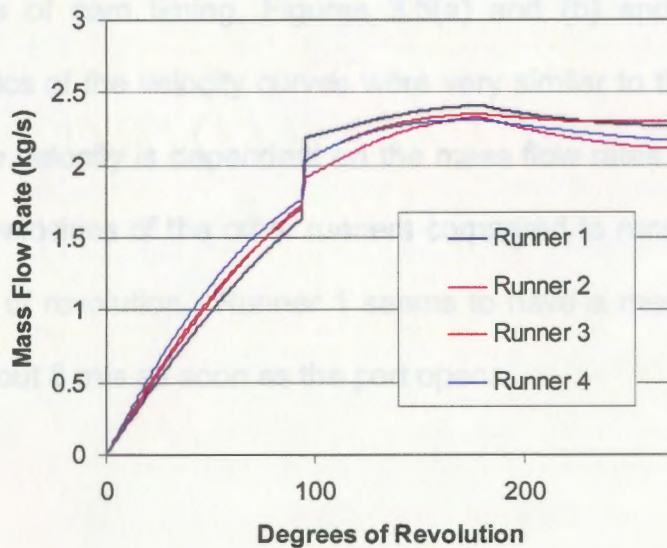
For the unsteady analysis the valves must be open and closed with respect to the engine rotation. By looking at Table 3.1 it can be seen that there are only eight different possibilities of the valves being open or closed. So for the transient study the boundary conditions for each stage were created. Then using a journal file each boundary condition file was loaded at the timestep corresponding to the degree in which it was active. Once the stage was over the next set of boundary conditions was loaded and was run for the appropriate length of timesteps. This was done for two complete revolutions in order to check for any variance between the revolutions; there was not any. The mass flow rates and velocity for the runners and inlet were stored in a monitor file and then read into Excel, where they were more easily analyzed and compared to each other.

The mass flow rates were graphed in the actual timing and also based on the degrees of cam timing (Figures 3.3a and b) so they could be compared in an easier manner. In Figure 3.3a, it can be seen that all of the cylinders behave in a similar manner. The mass flow rate increases from zero when the port is first opened. The rate jumps dramatically when the other port closes and continues to increase to its peak until the next port opens. The mass flow rate then steadily decreases until the port closes. While the trends look the same there are some differences which are more easily seen in Figure 3.3b. During the first 94 degrees that the valve is open, another valve is open as well. During this time, runner 4, the runner closest to the throttle body has the greatest amount of flow. For the next 86 degrees the greatest amount of air flows into the port because

the valve is open all by itself where runner 1 has the largest amount, with 3 and 4 very close to each other. For the remainder of the cams rotation, the next valve just begins to open. During this time, runner 1 and 3 have flow more than 2 and 4. These can all be seen quite clearly in Figure 3.4.



(a)



(b)

Figure 3.3: Mass Flow Rate with respect to (a) Engine Timing, (b) Cam Timing

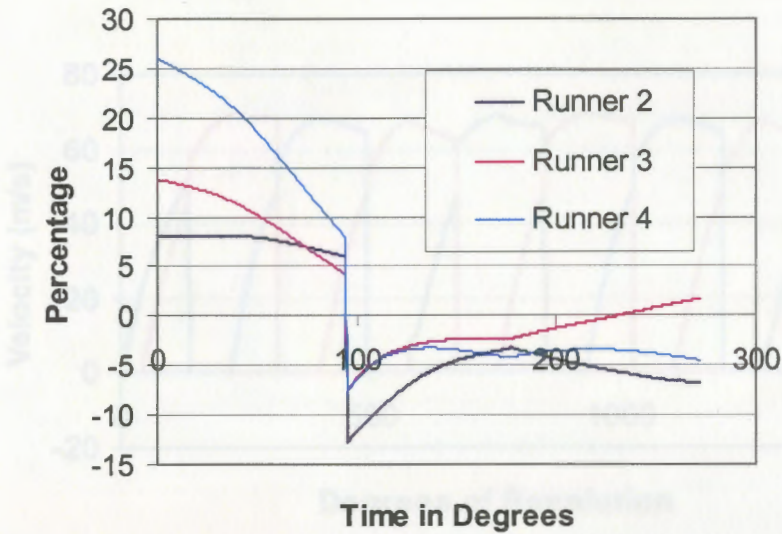


Figure 3.4: Mass Flow Rate as Compared to Runner 1 with respect to Cam Timing

The outlet velocities were also graphed in the actual timing and based on the degrees of cam timing, Figures 3.5(a) and (b) and 3.6. Note that the characteristics of the velocity curves were very similar to those of the mass flow because the velocity is dependent on the mass flow rates. One interesting point is how the velocities of the other runners compared to runner 1 at the in the first 20 degrees of revolution. Runner 1 seems to have a much higher velocity and jumps to about 8 m/s as soon as the port opens.

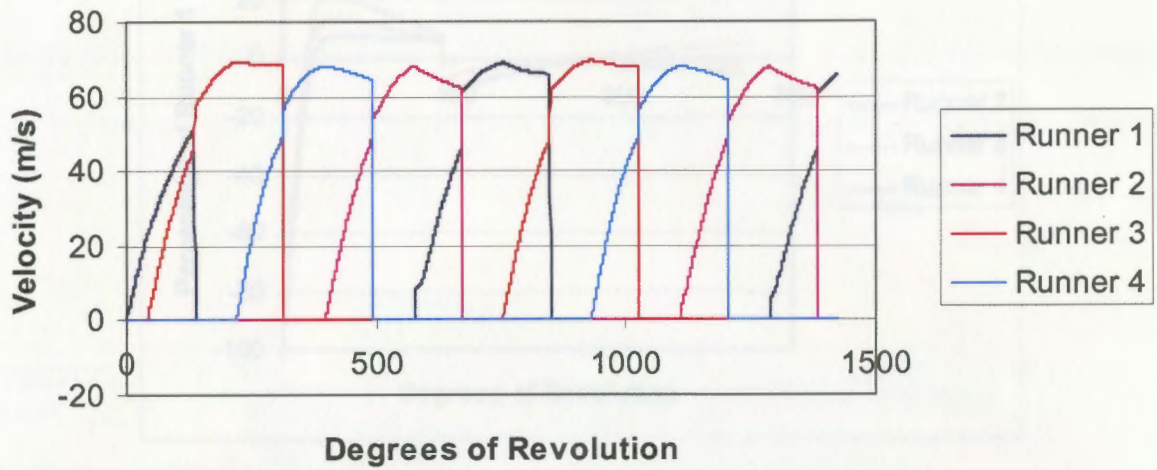
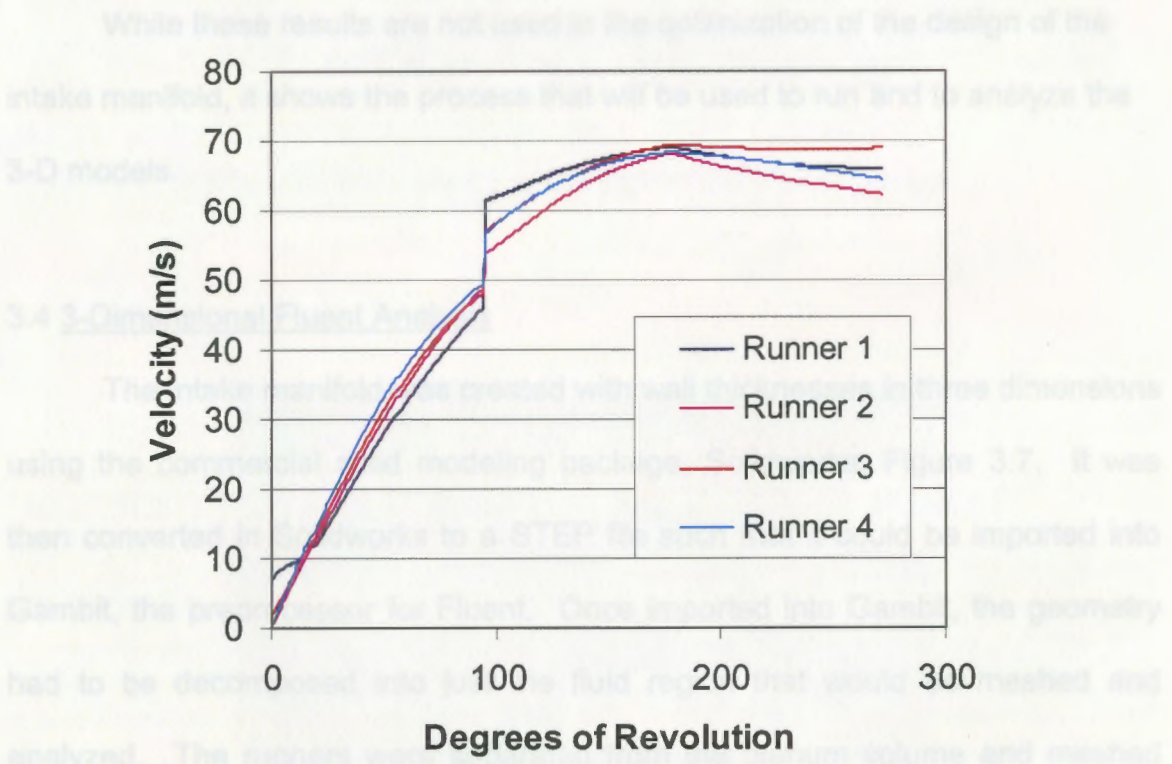


Figure 3.5: Velocities with respect to (a) Engine Timing, (b) Cam Timing

(a)



(b)

Figure 3.5: Velocities with respect to (a) Engine Timing, (b) Cam Timing

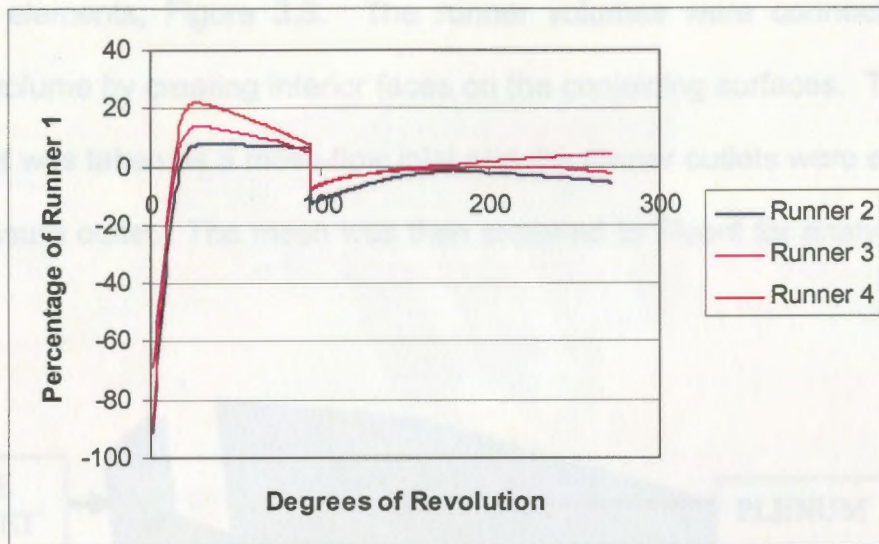


Figure 3.6: Velocities as Compared to Runner 1 with respect to Cam Timing

While these results are not used in the optimization of the design of the intake manifold, it shows the process that will be used to run and to analyze the 3-D models.

3.4 3-Dimensional Fluent Analysis

The intake manifold was created with wall thicknesses in three dimensions using the commercial solid modeling package, Solidworks, Figure 3.7. It was then converted in Solidworks to a STEP file such that it could be imported into Gambit, the preprocessor for Fluent. Once imported into Gambit, the geometry had to be decomposed into just the fluid region that would be meshed and analyzed. The runners were separated from the plenum volume and meshed using a Cooper hexahedral mesh while the plenum meshed with a mixed tetrahedral/hexahedral mesh. The full 3D model consisted of approximately

180,000 elements, Figure 3.8. The runner volumes were connected to the plenum volume by creating interior faces on the adjoining surfaces. The throttle body inlet was taken as a mass-flow inlet and the runner outlets were either walls or a pressure outlet. The mesh was then exported to Fluent for analysis, Figure 3.9.

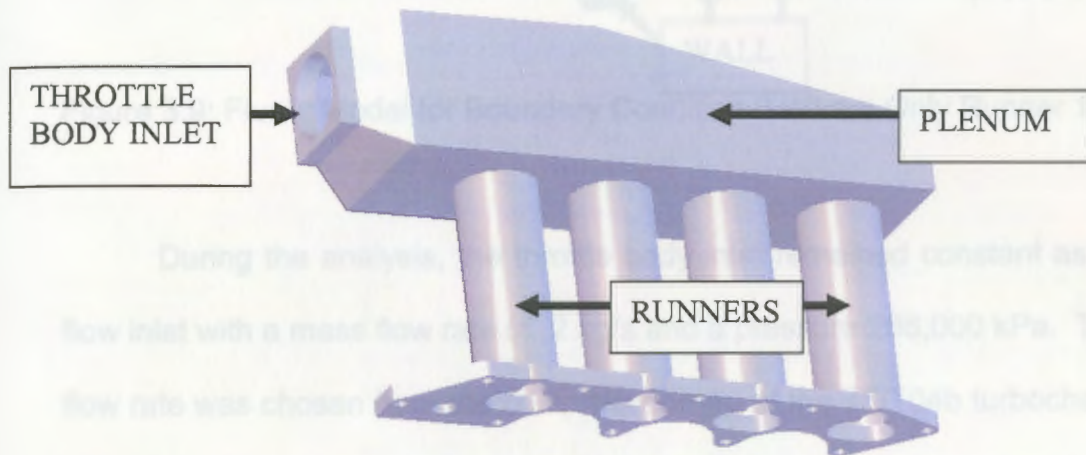


Figure 3.7: Solidworks Solid Model of the Optimized Model Design

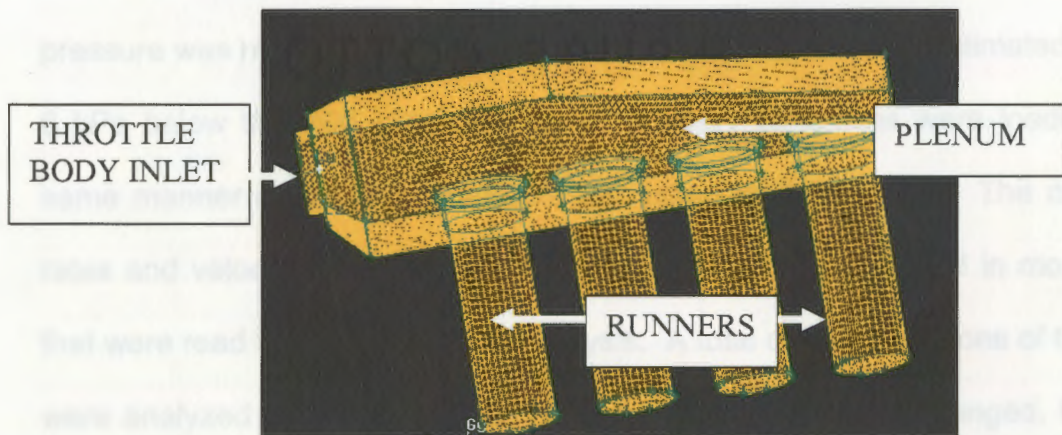


Figure 3.8: Meshed Gambit Model Showing Fluid Volumes

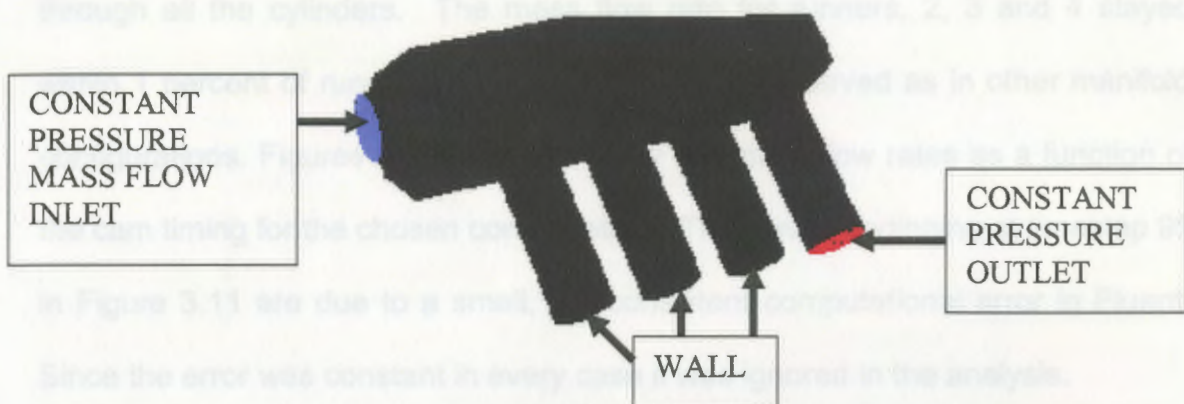


Figure 3.9: Fluent Model for Boundary Condition 0 Where Only Runner 1 is Open

During the analysis, the throttle body inlet remained constant as a mass-flow inlet with a mass flow rate of .2 kg/s and a pressure 206,000 kPa. The mass flow rate was chosen from the compressor map of the T3/T04b turbocharger that has an estimated mass flow rate of .2 kg/s at 1bar gauge pressure. It must be noted that pressure had no effect on the mass flow rate distribution to the runners. The runner outlets were either a pressure outlet of 200,000 kPa or a wall depending on the boundary conditions that were loaded. The exact pressure was not known at the runner outlets, therefore it was estimated at about 6 kPa below the inlet pressure. The boundary conditions were loaded in the same manner as the 2-D model as discussed in Section 3.3. The mass flow rates and velocities through the inlet and outlets were recorded in monitor files that were read into Excel for data analysis. A total of nine variations of the model were analyzed with the variables h , b , and y parametrically changed, Fig. 3.10. These variations, and the subsequent differences in runner mass flow rates, are summarized in Table 3.2. The model with the variable b equal to 6 inches, y

equal to 2, and h equal to 1 produced the most equal distribution of the flow through all the cylinders. The mass flow rate for runners, 2, 3 and 4 stayed within 1 percent of runner 1, and runner 4 was not starved as in other manifold configurations. Figures 3.11 and 3.12 show the mass flow rates as a function of the cam timing for the chosen configuration. The waves beginning at timestep 95 in Figure 3.11 are due to a small, but consistent computational error in Fluent. Since the error was constant in every case it was ignored in the analysis.

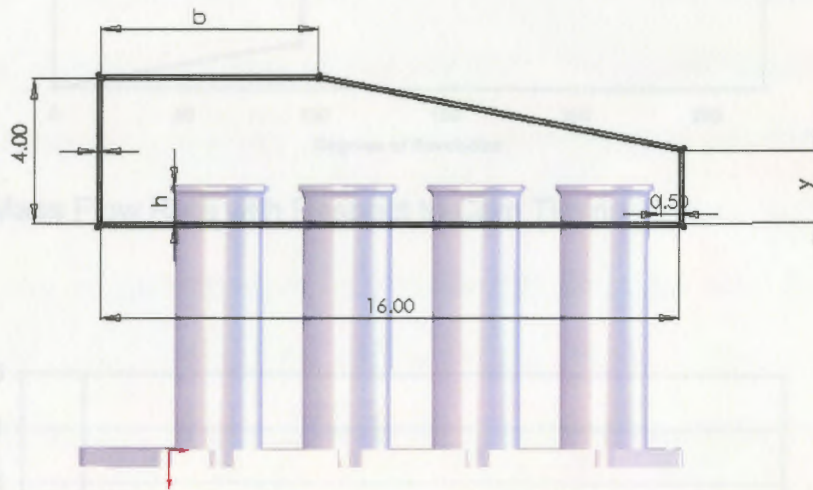


Figure 3.10: Plenum Dimensions for Optimized Manifold

Table 3.2: Results of Flow Rate Differences for the Nine Manifold Configurations

Manifold Configuration	Height Variables			Average Percent Difference of Runner 1		
	b	h	y	Runner 2	Runner 3	Runner 4
1	8	1	2.5	-2.1	1.2	-3.3
2	6	1	2.5	-2.4	0.8	-2.7
3	4	1	2.5	-1.9	0.9	-3.4
4	8	1	2	-1.5	1.1	-2.4
5	6	1	2	-0.9	0.7	-1.9
6	4	1	2	-1.1	0.8	-1.8
7	8	0.5	2	-1.7	1.0	-3.4
8	6	0.5	2	-1.3	0.7	-2.2
9	4	0.5	2	-1.2	0.6	-4.0

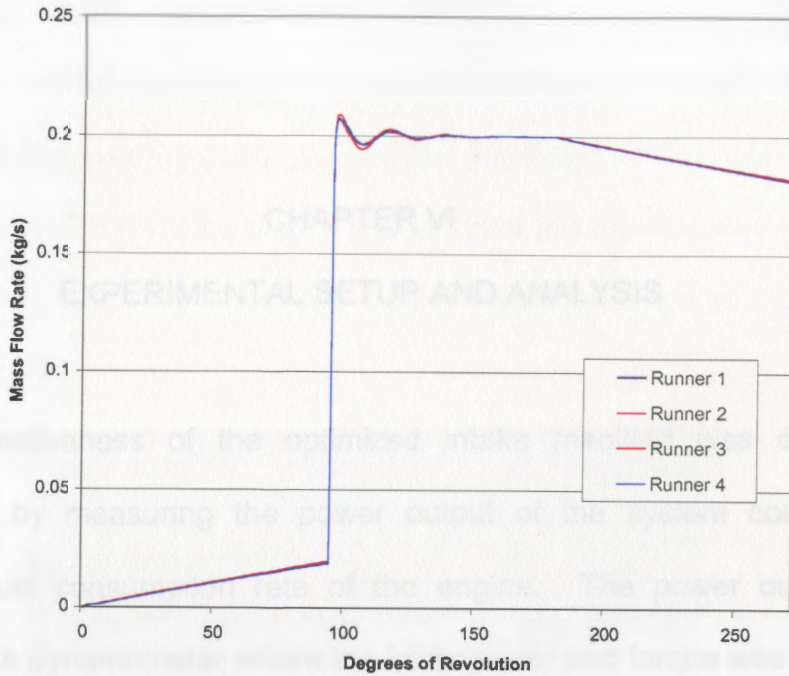


Figure 3.11: Mass Flow Rate with Respect to Cam Timing

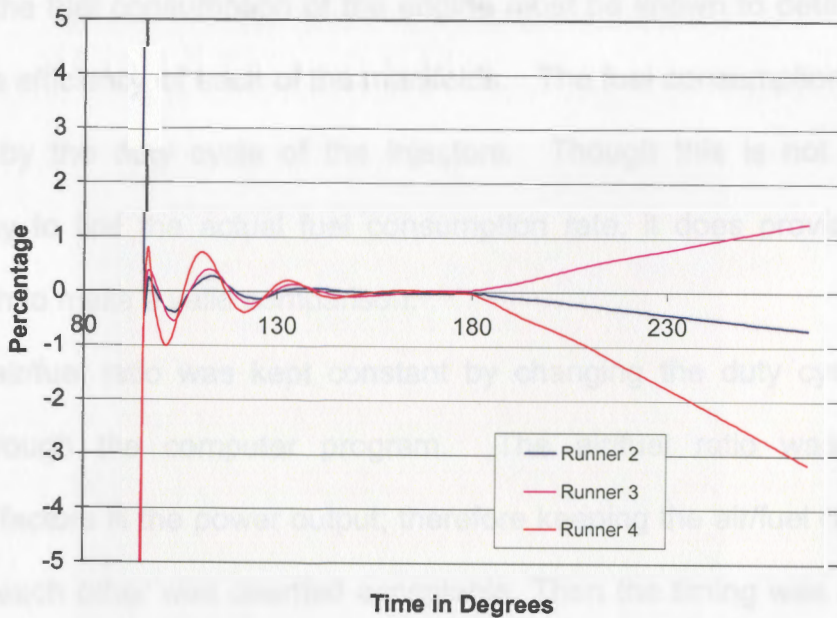


Figure 3.12: Mass Flow Rate as Compared to Runner 1 with Respect to Cam Timing

4.1 Experimental Setup

The test bed for the intake manifold comparison was a 1994 Honda Civic with a modified B-series turbocharged 1637cc 4-cylinder engine with an intake GSR VTEC head. The engine with the stock variable geometry intake and then

CHAPTER VI

EXPERIMENTAL SETUP AND ANALYSIS

The effectiveness of the optimized intake manifold was determined experimentally by measuring the power output of the system coupled with knowing the fuel consumption rate of the engine. The power output were determined by a dynamometer where the horsepower and torque was measured by determining the resistance placed against a large rotating drum. While the overall effectiveness of the optimized intake manifold could be seen from the dyno plots, the fuel consumption of the engine must be known to determine the ascertain the efficiency of each of the manifolds. The fuel consumption rate was determined by the duty cycle of the injectors. Though this is not the most accurate way to find the actual fuel consumption rate, it does provide results close enough to make a valid comparison.

The air/fuel ratio was kept constant by changing the duty cycle of the injectors through the computer program. The air/fuel ratio was not the determining factors in the power output; therefore keeping the air/fuel ratio within .3 points of each other was deemed acceptable. Then the timing was advanced as far as possible for both manifolds until knock set in. With greater volumetric efficiency, less timing should be needed to reach maximum power.

4.1 Experimental Setup

The test bed for the intake manifold comparison was a 1994 Honda Civic with a modified B-series turbocharged 1837cc 4-cylinder engine with an Integra GSR VTEC head. The engine was first fitted with the stock variable geometry intake and then with the optimized intake manifold, Figures 4.1 and 4.2, respectively.



Figure 4.1: Stock Variable Geometry Acura Integra GSR Intake Manifold



Figure 4.2: Optimized Intake Manifold on the Car

The engine was controlled by the modified stock engine control unit (ECU). The modified ECU was equipped with a realtime standalone engine management system, Crome. Using this program, the operator has the ability to change the engine's running characteristics, which are then reflected immediately. The ECU has the ability to send all of the engine's parameters to a laptop via a serial port. The laptop sends the changed data back to the ECU in real-time via its USB port though the romulator (Ostrich). Therefore any changes made to the fuel and ignition maps were immediately changed on ECU. Referring to the schematic of the data acquisitions setup, Figure 4.3, the interaction between the ECU and the user was as follows.

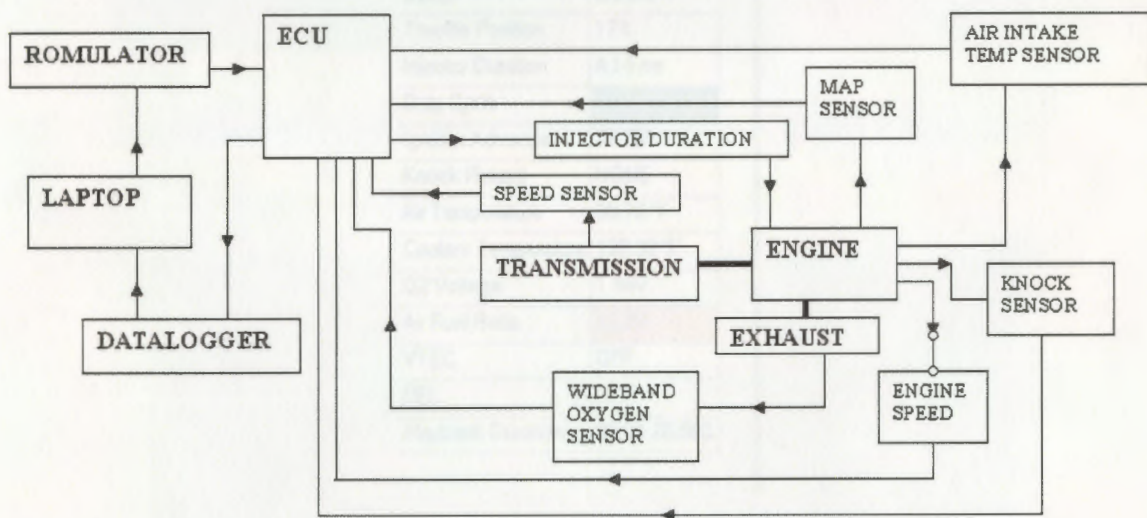


Figure 4.4 – Sensor Parameters That were Logged

Figure 4.3 – Engine Control Schematic

The ECU received engine performance conditions from the sensors, such as the manifold absolute pressure (map), and air intake temperature that were determined from a pressure transducer and a thermocouple respectively, Figure 4.4. The ECU also received engine speed from the crank position sensor in the

distributor, the vehicle speed from a rotational sensor on the differential, and the air/fuel ratio from a PLX wideband oxygen sensor to ensure accurate readings. There was also a knock sensor which was a piezoelectric sensor that detects predetonation. Basically this was a microphone tuned to hear the frequencies of knock. All sensor data was sent back to the ECU and to the operator through a datalogging port. Thus, the operator could change the injector duration and ignition advance based on the previously mentioned parameters.

Data Type	Value
Engine Speed	2640 rpm
Vehicle Speed	38.4 Mph
Gear	4
Manifold Pressure	604 mbar
Boost	0.0 psi
Throttle Position	17%
Injector Duration	4.14 ms
Duty Cycle	9%
Ignition Advance	25.75°
Knock Retard	NONE
Air Temperature	50.72 °F
Coolant Temperature	135.32 °F
O2 Voltage	1.94V
Air Fuel Ratio	13.70
VTEC	OFF
CEL	OFF
Playback Duration	00:04:26.563

Figure 4.4— Sensor Parameters That were Logged

The data acquisition also provides fuel and ignition data via tables. The fuel table was a matrix of values representing the duty cycle of the injectors based on RPM from the crank angle sensor and pressure from the MAP sensor. The fuel tables could be viewed in tabular data, graphical representation or actual duty cycle of the injectors, Figures 4.5, 4.6, and 4.7 respectively. The

ignition tables could also be viewed in a tabular format or in the graphical mode, Figures 4.8, 4.9.

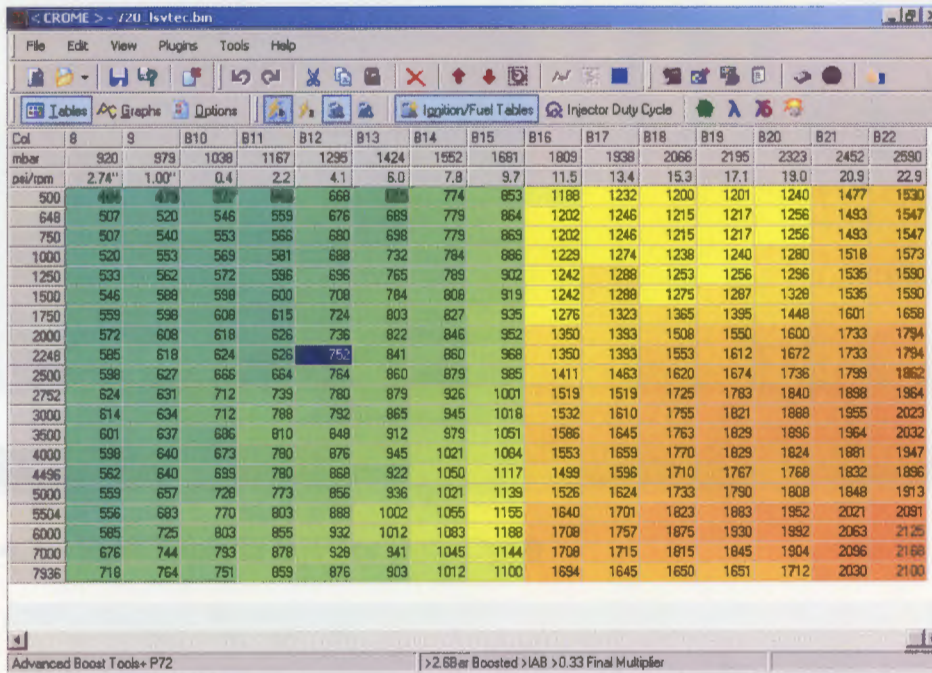


Figure 4.5 – Fuel Table in Tabular Format

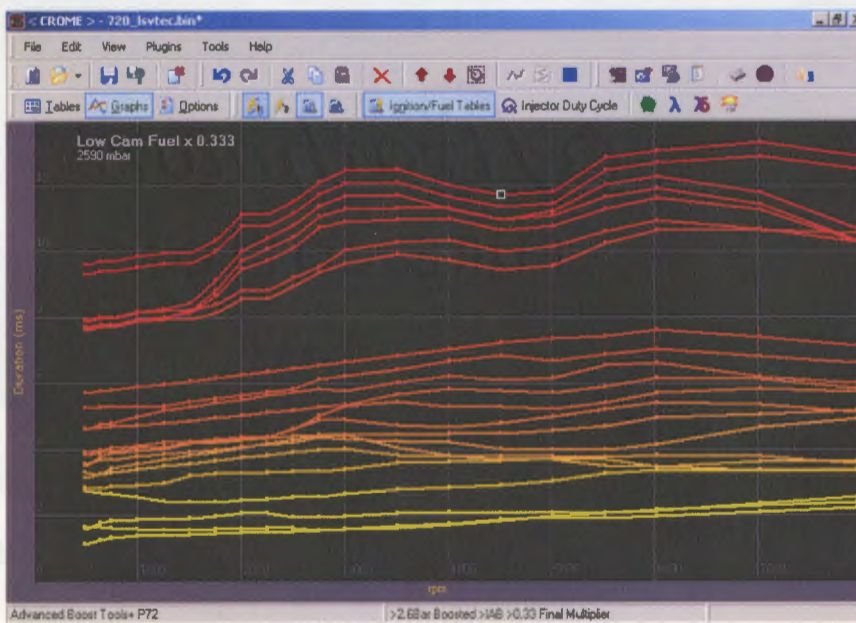


Figure 4.6 – Fuel Table in Graphical mode

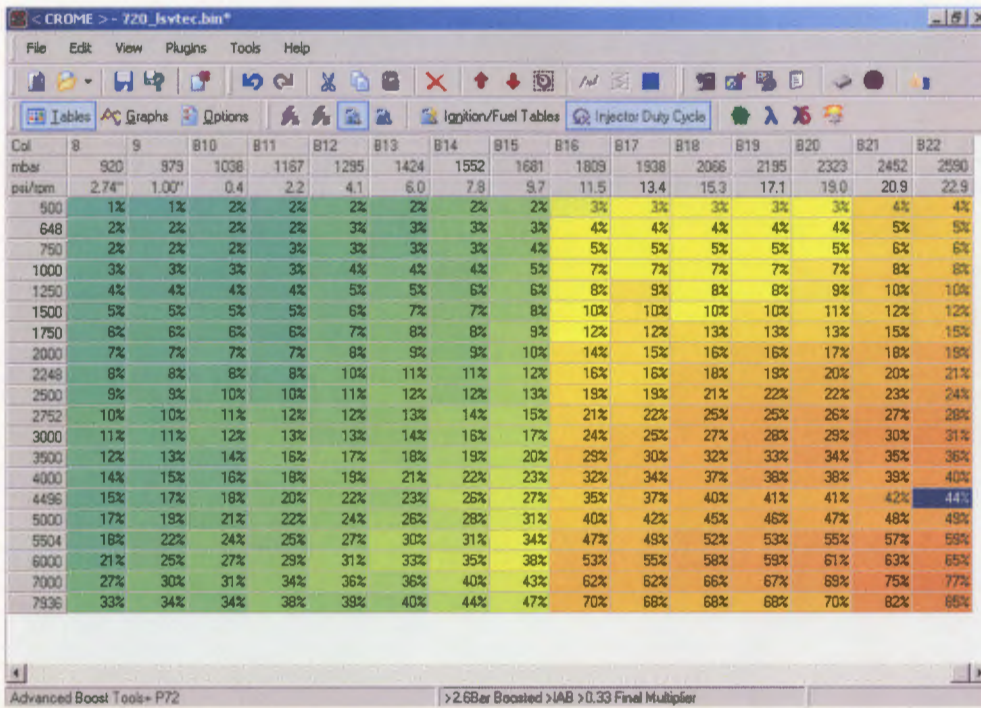


Figure 4.7 – Fuel Table in Injector Duty Cycle

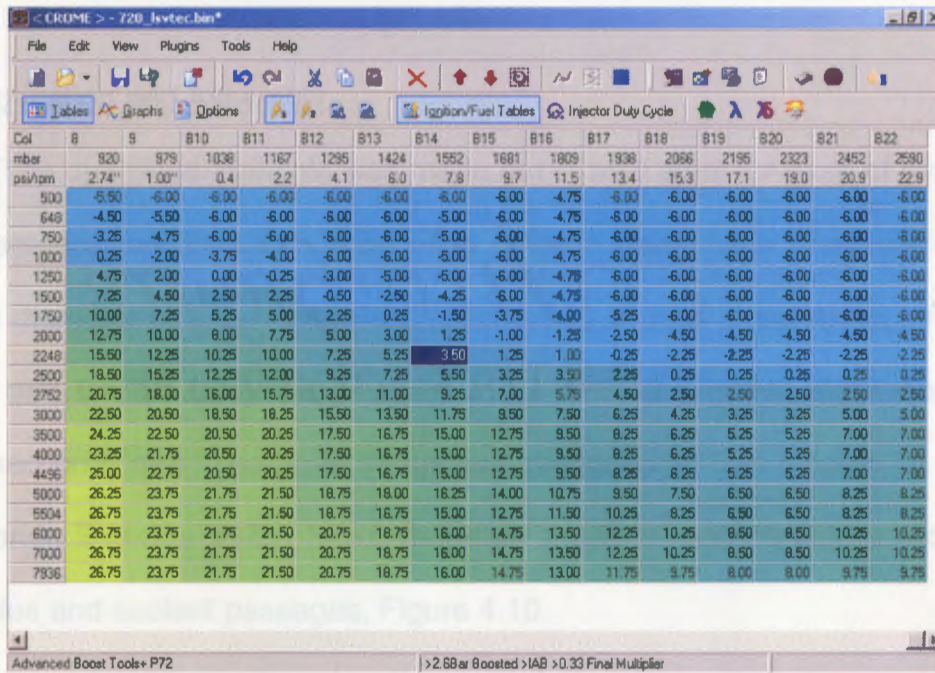


Figure 4.8 – Ignition Table in Tabular Format

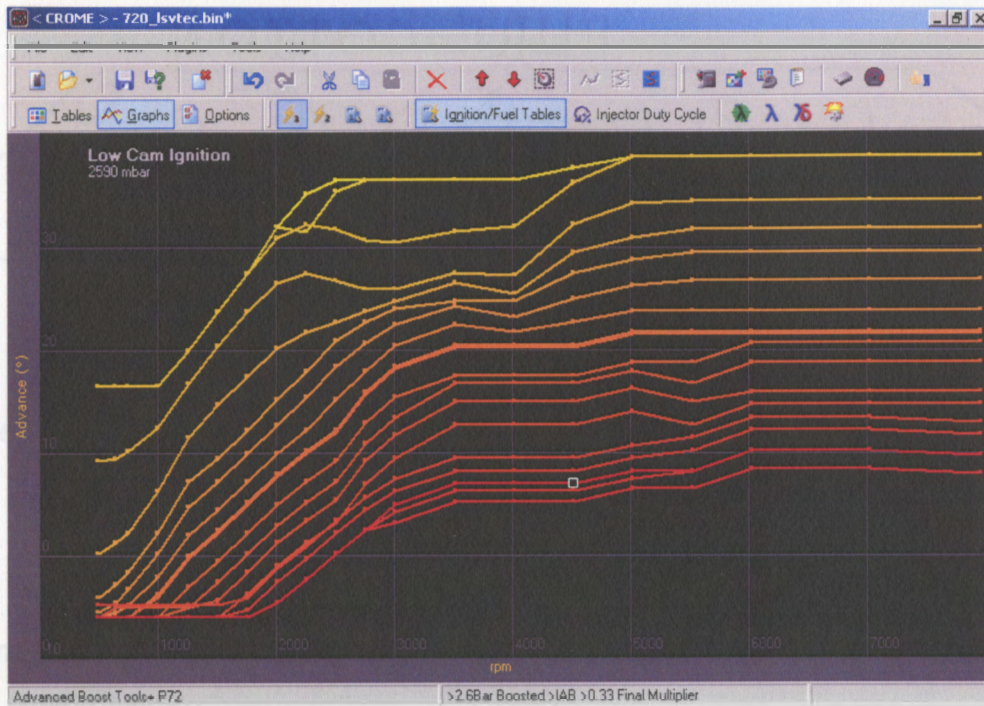


Figure 4.9– Ignition Table in Graphical Mode

4.2 Fabrication and Assembly

The optimized manifold was made out of mild steel for ease of availability, manufacturing, welding, and cost. The runners were made from .049 in thick, 2.25 in diameter pipe and the plenum from .049 in thick sheet metal. The head flange and throttle body flange were made from 0.5 in flat stock and were machined on a mill. The head flange was designed so that it could be used on any Honda B-series VTEC head, therefore it had to accommodate two sets of bolt holes and coolant passages, Figure 4.10.

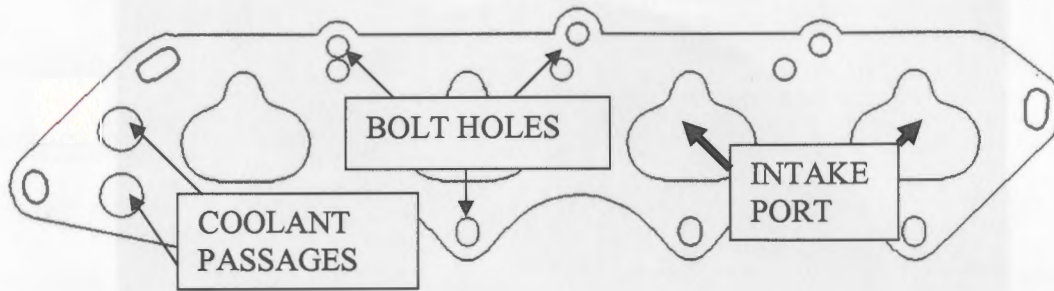


Figure 4.10: Head Flange That Fits All VTEC Heads

The 2.25 in diameter runners were flared at the top of the runner, Figure 4.11, to a 0.25 in radius which is between 20 and 25% of the runner radius as per Vorum, 1980. A bell shaped entrance was also proved beneficial by Tallio et al, 1993. The Venturi entrance was created using a custom press tool. The runners were welded in the plenum 1 inch from the base, which was determined in Section 3.4. The runners had to be tapered down to the right size of the intake port. To do so, a 2.75 in deep pie cut was removed from the runners, so that the runners could be matched to the intake ports, Figure 4.12.

Figure 4.12: Runner Taper Welded to Head Flange

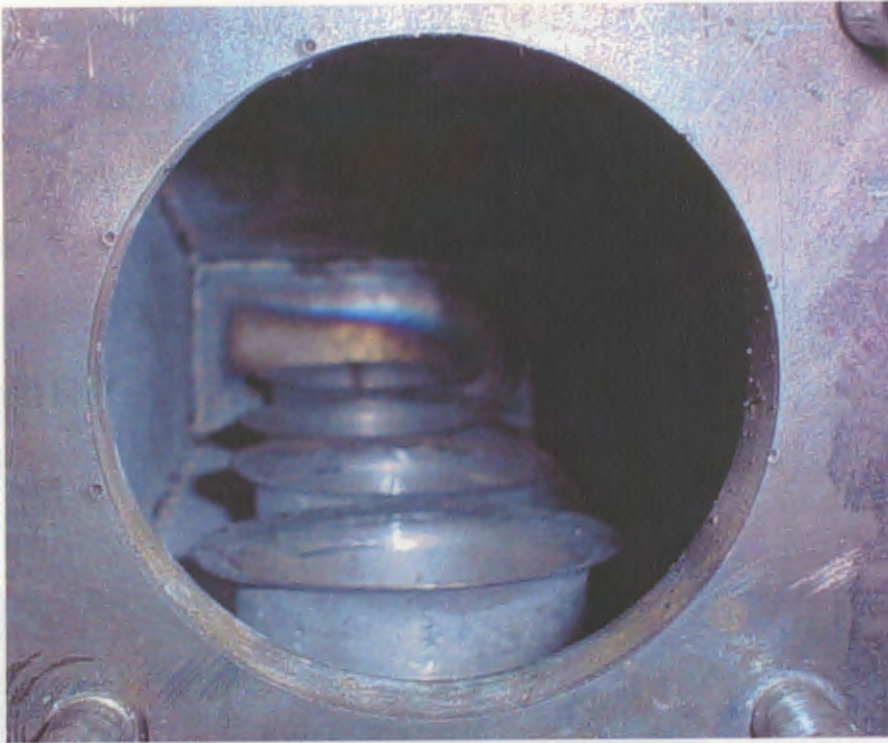


Figure 4.11: Fluted Venturi's on Runner Entrance



Figure 4.12: Runner Taper Welded to Head Flange

Another improvement to the intake manifold was removing the idle air control valve from the intake manifold (IACV). The IACV is a solenoid that meters the amount of air into the intake manifold while the throttle plate is closed during idle. This was removed for two reasons: (1) the IACV air passage is cast into the stock manifold thereby making it quite difficult to accommodate in a sheet metal intake, and (2) the IACV carries coolant through it, effectively heating the manifold. Therefore, the IACV was mounted remotely off of the intake manifold and placed on the fire wall, Figure 4.13.

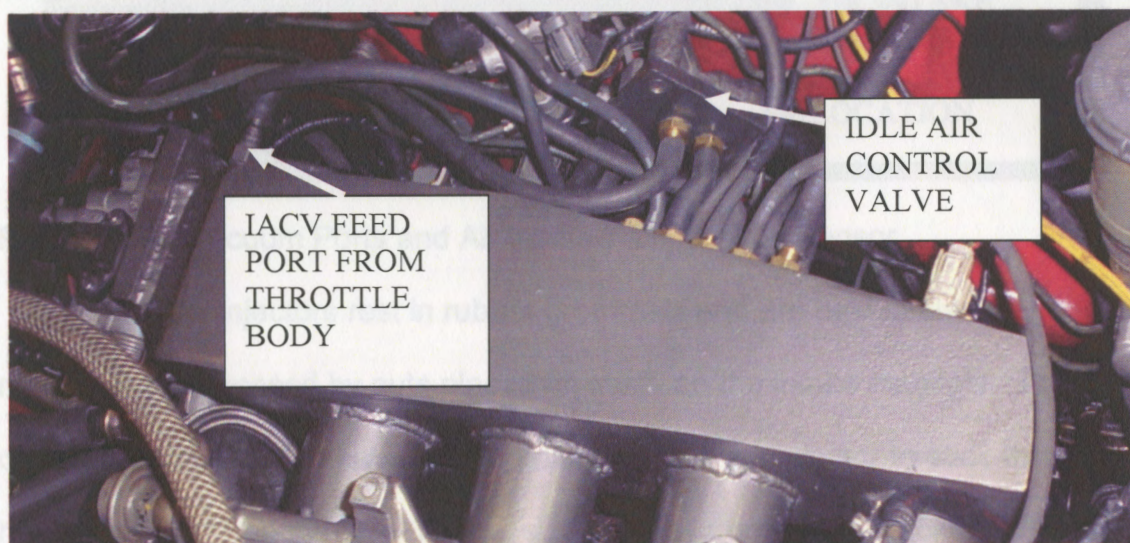


Figure 4.13: The Remote Mounted Idle Air Control Valve

Another advantage to the optimized manifold is the plethora of vacuum ports available. The stock manifold has approximately 4 vacuum ports. Once a turbocharger is installed, more vacuum ports are required for the blow-off valve, the wastegate, the boost controller, and the boost gauge. With the stock manifold to accommodate these needs, the already dedicated lines must be teed off. Not only does this clutter the engine bay, but it also reduces the signal

strength to all of the teed devices. To solve this problem, 10 vacuum ports were installed in the back of the optimized manifold on the sloped portion, Figure 4.14, to give the maximum amount of room once installed in the engine bay. The air intake temperature sensor was also installed on the sloped portion, Figure 4.14.

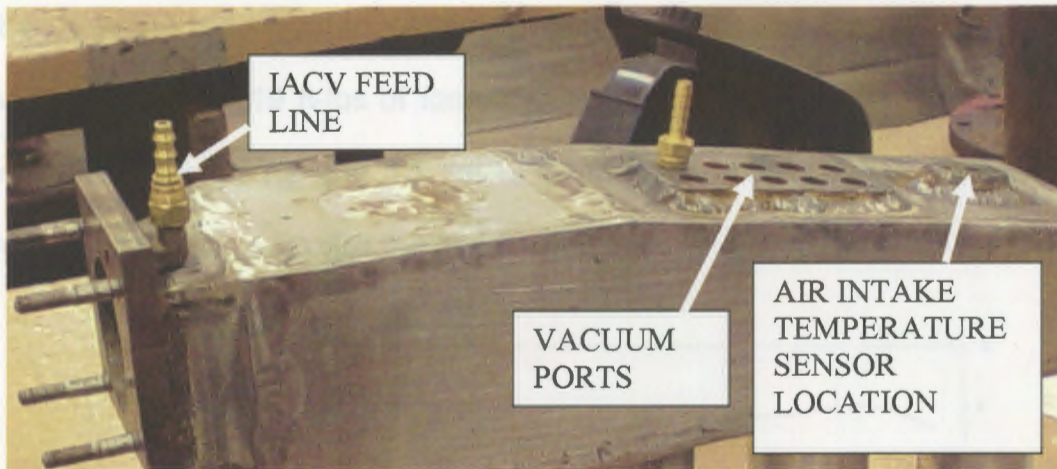


Figure 4.14: Vacuum Ports and Air Intake Temperature Sensor

The fuel injectors rest in rubber grommets and are held in place by the fuel rail that is compressed by nuts placed on studs on the intake manifold. To do the cylindrical stock had to have a hole drilled in it for the injector to stick through. A hole was then countersunk to the size of the grommets. Brackets were also made to place the injectors at a stock angle of 54 degrees, using the stock fuel rail and fuel pressure regulator that were used in the testing of both manifolds.

Figure 4.15: Power Output for Stock Manifold vs. Boost Pressure

4.3 Stock Manifold Results

The test car with the stock manifold was run on a Dynojet 248 chassis dynamometer on March 28th, 2006 at Akron Horse power in Akron, OH. The ambient air temperature was approximately 50-55 °F and the humidity was 35%.

The fuels maps were already optimized with an air/fuel ratio of 11.6-11.8 beforehand so that the time spent on the dynamometer could be used to extract the maximum power by experimenting with the timing advance and VTEC engagement. All pulls on the dyno where done in 4th gear as it has the closest 1:1 ratio in the transmission. After approximately 10 runs, the maximum power was reached with 219 ft-lbs of torque and 272 horsepower with the boost level fluctuating between 7.8 and 8.8 psi. Figure 4.15 shows the results; notice the how the torque curve mimics the boost level.

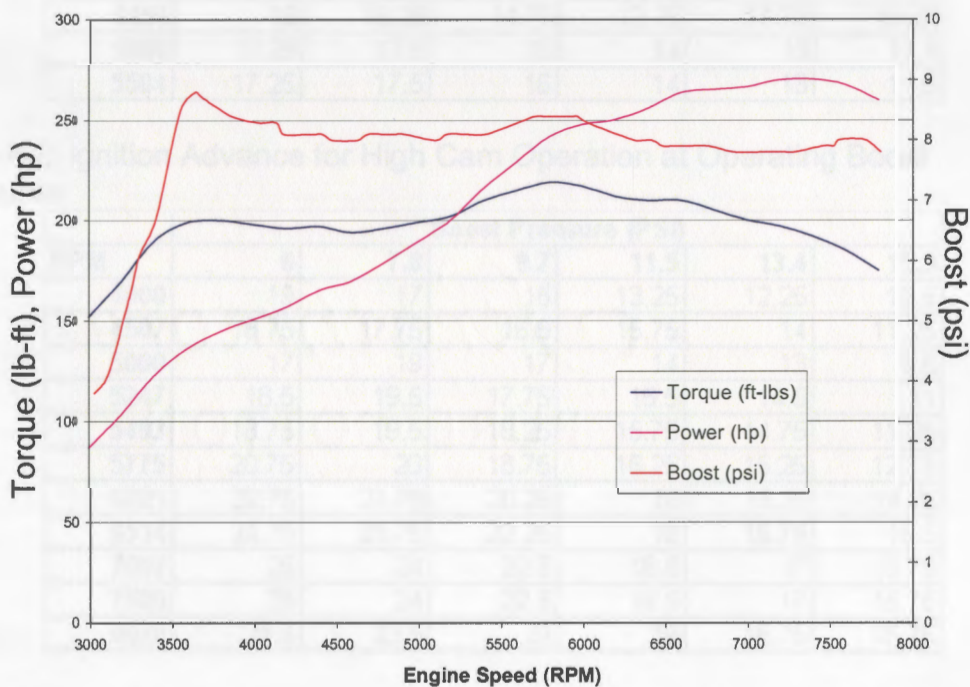


Figure 4.15: Power Output for Stock Manifold vs. Boost Pressure

The way to extract maximum power from an engine is to advance timing until power starts to fall off or stops increasing. At this point the knock threshold has been reached, therefore the correct procedure is back the timing down to

where it stopped increasing power. This is now the safest, most powerful tune that the engine can make. Tables 4.1 and 4.2 show the ignition advance for boost levels beyond 6 psi and rpms from 3000-8000 for both the low and high cam. At 7.8 psi on the high cam, the engine required about 24 degrees of advance above 6000 rpm.

Table 4.1: Ignition Advance for Low Cam Operation at Operating Boost Pressures

RPM	Boost Pressure (PSI)					
	6	7.8	9.7	11.5	13.4	15.3
3000	14	14.25	12.75	10.75	9.25	8.25
3500	16	16.25	14.75	12.75	11.25	10.25
4000	16	16.25	14.75	12.75	11.75	10.25
4496	16	16.25	14.75	12.75	11.75	10.25
5000	17.25	17.5	16	14	13	11.5
5504	17.25	17.5	16	14	13	11.5

Table 4.2: Ignition Advance for High Cam Operation at Operating Boost Pressures

RPM	Boost Pressure (PSI)					
	6	7.8	9.7	11.5	13.4	15.3
4000	19	17	15	13.25	12.25	10.5
4507	18.75	17.75	16.5	15.75	14	11.25
5000	17	19	17	14	13	9.5
5247	18.5	19.5	17.75	15.5	14.5	11
5493	18.75	19.5	18.25	15.75	14.75	11.25
5775	20.75	20	18.75	16.25	15.25	12.75
6021	22.75	21.75	20.25	16	15.25	14.25
6514	24.75	23.75	22.25	18	16.75	15.5
7007	25	24	22.5	18.5	17	15.75
7500	25	24	22.5	18.5	17	15.75
8028	24.5	23.5	22	18	16.75	15.75

The fuel tables were adjusted before the dyno session to achieve a constant 11.6-11.8 air/fuel ratio. Timing will only effect air/fuel ratios slightly, therefore they required very little attention during the tuning session. Injector duty cycle graphs for higher boost pressures are given in Tables 4.3 and 4.4.

Also a VTEC engagement point of 5500 rpm yielded the most mid-range power and flattest torque curve.

Table 4.3: Injector Duty Cycle for Low Cam Operation at Operating Boost Pressures

RPM	Boost Pressure (PSI)					
	6	7.8	9.7	11.5	13.4	15.3
3000	16	18	18	18	20	21
3500	19	21	21	22	24	25
4000	22	23	25	25	28	30
4496	24	27	28	29	31	33
5000	28	31	32	33	36	37
5504	32	34	35	38	39	42

Table 4.4: Injector Duty Cycle for High Cam Operation at Operating Boost Pressures

RPM	Boost Pressure (PSI)					
	6	7.8	9.7	11.5	13.4	15.3
4000	24	24	27	28	30	31
4507	26	26	29	31	33	34
5000	29	29	33	36	38	39
5247	31	32	36	38	40	41
5493	33	34	37	39	42	42
5775	35	36	39	40	45	46
6021	37	39	40	42	46	48
6514	40	41	44	47	51	52
7007	43	44	48	51	54	56
7500	45	47	51	53	58	59
8028	48	51	55	59	61	63

4.3 Optimized Manifold Results

The test car with the optimized manifold was tested on dynamometer on April 7th, 2006 also at Akron Horse power in Akron, OH. The ambient air temperature was approximately 70 °F and the humidity was 100%, as it was raining outside and the garage doors must be open to vent exhaust gases. Again the fuels maps were already optimized so that the time spent on the

dynamometer could be used to extract the maximum power by experimenting with the timing advance and VTEC engagement. After 7 runs, the maximum power was reached with 212 ft-lbs of torque and 275 horsepower with the boost level fluctuating between 7.5 and 9.1 psi. Figure 4.16 shows the results; notice how the boost falls below 8 psi above 5000 rpm. The optimal VTEC engagement point was reached at 5200 rpm.

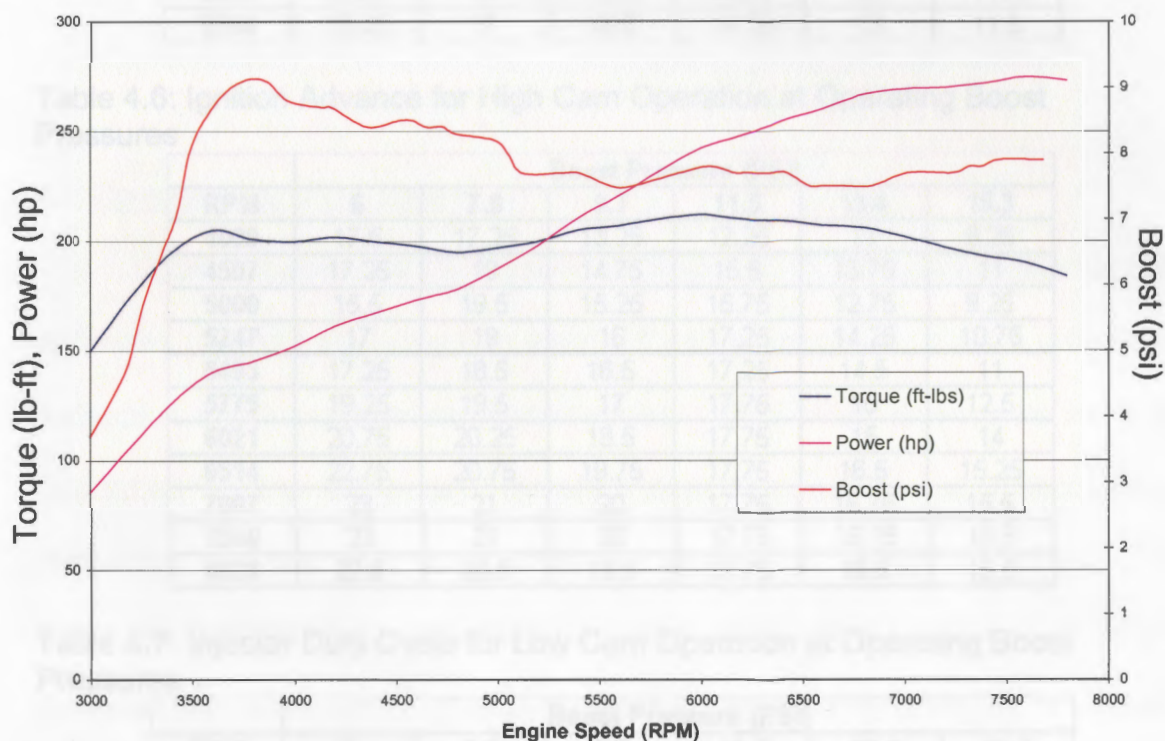


Figure 4.16: Power Output for Optimized Manifold vs. Boost Pressure

The ignition timing and fuel injector duty cycle was determined in the same process outlined in Section 4.2. With the new manifold the engine reached maximum power output above 6000 rpm with about 21 degrees of ignition advance, Tables 4.5 and 4.6. The injector duty cycle tables for the low and high

cam, Tables 4.6 and 4.7 respectively, show the amount of fuel the optimized manifold required.

Table 4.5: Ignition Advance for Low Cam Operation at Operating Boost Pressures

RPM	Boost Pressure (PSI)					
	6	7.8	9.7	11.5	13.4	15.3
3000	14.25	13.5	12.25	11	9.25	8.25
3500	16.25	16.5	15.25	13	11.25	10.25
4000	16.25	16.5	15.25	13.5	12.25	10.75
4496	17	17	16.25	13.5	12.25	10.75
5000	18.25	17	16.5	14.25	13	11.5
5504	18.25	17	16.5	14.25	13	11.5

Table 4.6: Ignition Advance for High Cam Operation at Operating Boost Pressures

RPM	Boost Pressure (PSI)					
	6	7.8	9.7	11.5	13.4	15.3
4000	17.5	17.25	13.25	12.25	11	9.25
4507	17.25	19	14.75	15.5	13.75	11
5000	15.5	19.5	15.25	15.75	12.75	9.25
5247	17	19	16	17.25	14.25	10.75
5493	17.25	18.5	16.5	17.25	14.5	11
5775	19.25	19.5	17	17.75	15	12.5
6021	20.75	20.25	18.5	17.75	15	14
6514	22.75	20.75	19.75	17.75	16.5	15.25
7007	23	21	20	17.75	16.75	15.5
7500	23	21	20	17.75	16.75	15.5
8028	22.5	20.5	19.5	17.75	16.5	15.5

Table 4.7: Injector Duty Cycle for Low Cam Operation at Operating Boost Pressures

RPM	Boost Pressure (PSI)					
	6	7.8	9.7	11.5	13.4	15.3
3000	15	17	18	19	19	20
3500	18	20	21	21	23	25
4000	20	22	23	24	27	28
4496	23	25	27	28	30	31
5000	25	28	30	32	34	35
5504	29	32	34	36	39	41

Table 4.8: Injector Duty Cycle for High Cam Operation at Operating Boost Pressures

RPM	Boost Pressure (PSI)					
	6	7.8	9.7	11.5	13.4	15.3
4000	19	21	24	28	31	32
4507	21	24	26	29	33	35
5000	23	27	30	29	34	36
5247	24	28	31	31	35	38
5493	27	30	33	34	39	41
5775	31	34	35	37	42	44
6021	34	35	37	40	43	45
6514	36	39	39	43	47	49
7007	39	40	43	46	50	52
7500	41	43	49	50	54	56
8028	43	45	52	55	57	59

4.4 Comparisons and Conclusions

Upon first glance at the horsepower and torque curves, it appears as if the optimized manifold produced less power all over powerband. It is not until closer inspection that the differences become clear. First of all, these tests were not performed on the same day, therefore one must consider the atmospheric conditions changed and the subsequent effects on the power output. The optimized manifold had more adverse conditions from the standpoint of oxygen available for combustion. This is because it was approximately 15 °F warmer and the humidity was 100%. The warmer the air, the less oxygen content; and the more humid the air; the less room for oxygen.

Another very notable observation and comparison comes from the boost curves shown for both manifolds in Figure 4.17. While the boost for the optimized manifold peaked higher, it fell below the stock manifold's boost above 5000rpm. This shows that the optimized manifold made nearly the same power

as the stock manifold with less boost, this is the optimized manifold design's first testament to its greater efficiency.

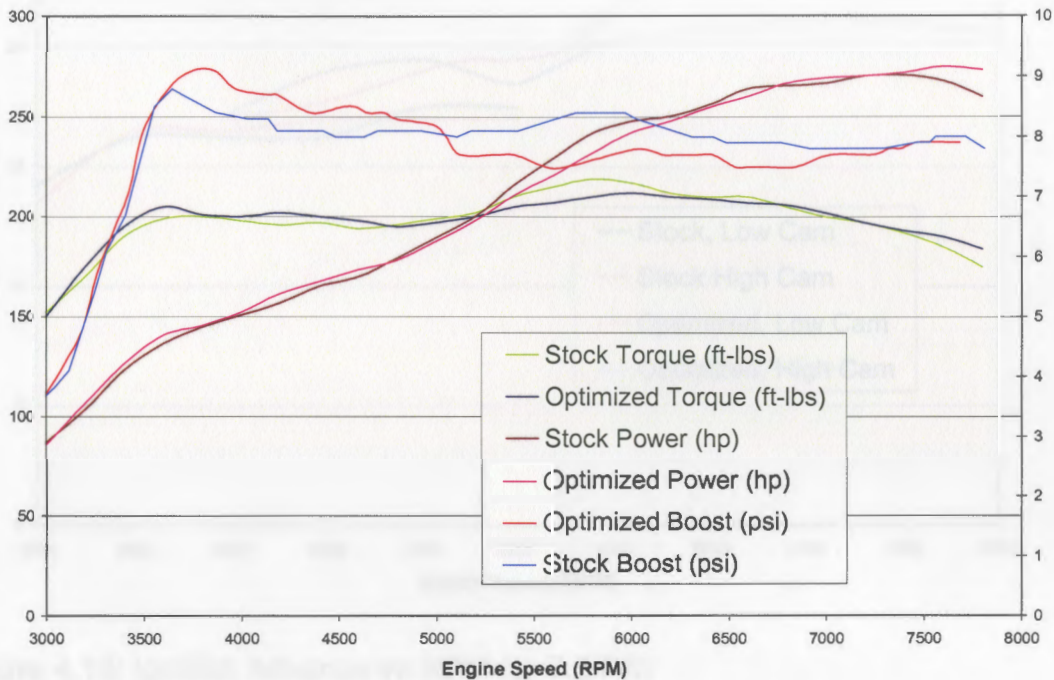


Figure 4.17: Power Output for Stock and Optimized Manifolds With Boost Pressure

The optimized manifold next displays its greater efficiency in its timing and fuel valves. Figure 4.18 shows the timing values for the 7.8 psi of boost across the powerband. The fact that the optimized manifold requires less total timing than the stock manifold above 5000 rpm is quite intriguing. Timing is a reflection of the efficiency of an engine cycle, the less timing that is required to reach peak power, the more efficient the cycle is. Below 5000 rpm the optimized intake needed more timing than the stock one.

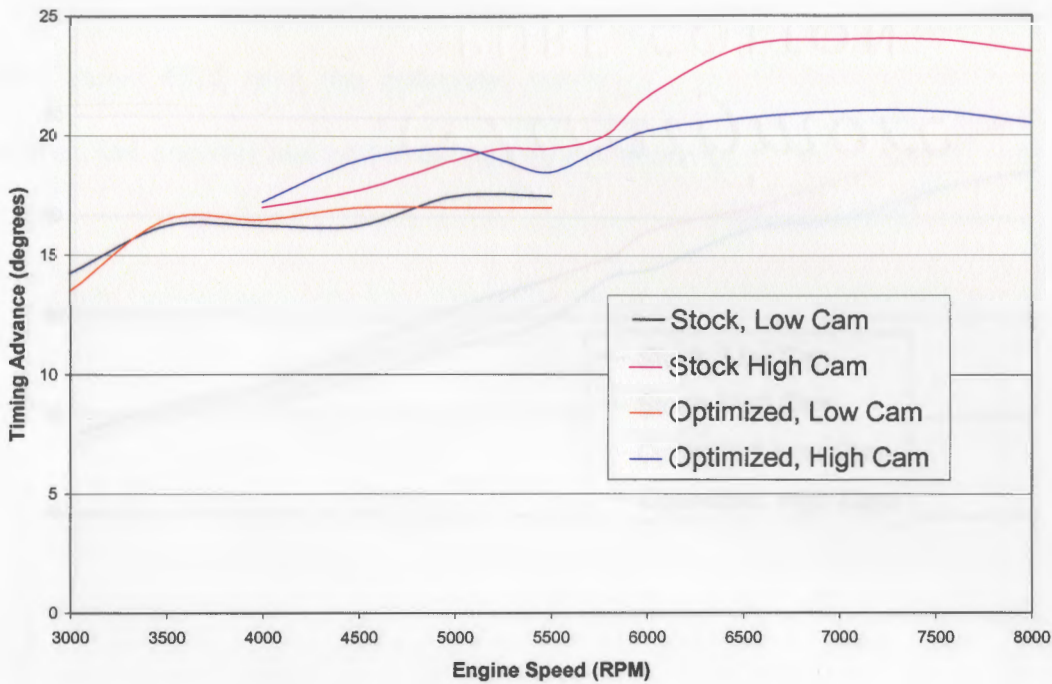


Figure 4.18: Ignition Advance vs RPM for 7.8 PSI

The duty cycle of the injectors also provides evidences of the efficiency of the optimized manifold. Both manifolds were tuned to a constant 11.6-11.8 air/fuel ratio, therefore an accurate comparison of the duty cycles could be made. Figures 4.19 and 4.20 demonstrate that the optimized cam required less fuel at the same 7.8 and 11.5 psi boost levels, respectively; again showing the greater efficiency of the optimized manifold. In fact the high cam required about 3% less fuel and the low cam about 1% less. This can also be seen in the previous Tables 4.3 and 4.4 for the stock design, 4.7, and 4.8 for the optimized design.

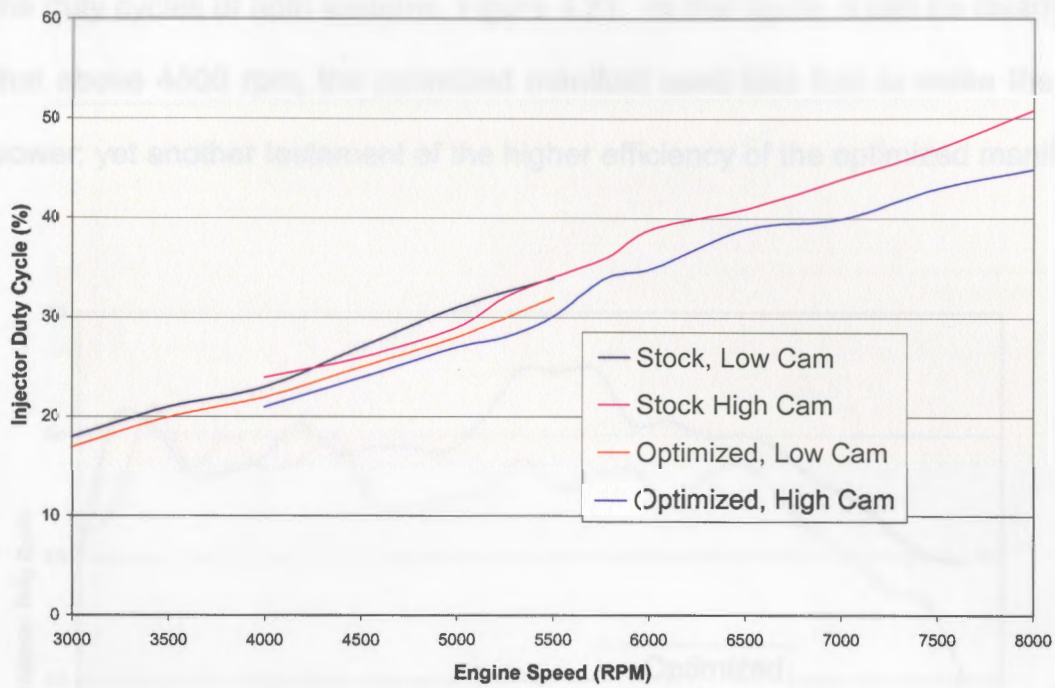


Figure 4.19: Fuel Injector Duty Cycle versus RPM for 7.8 psi Boost

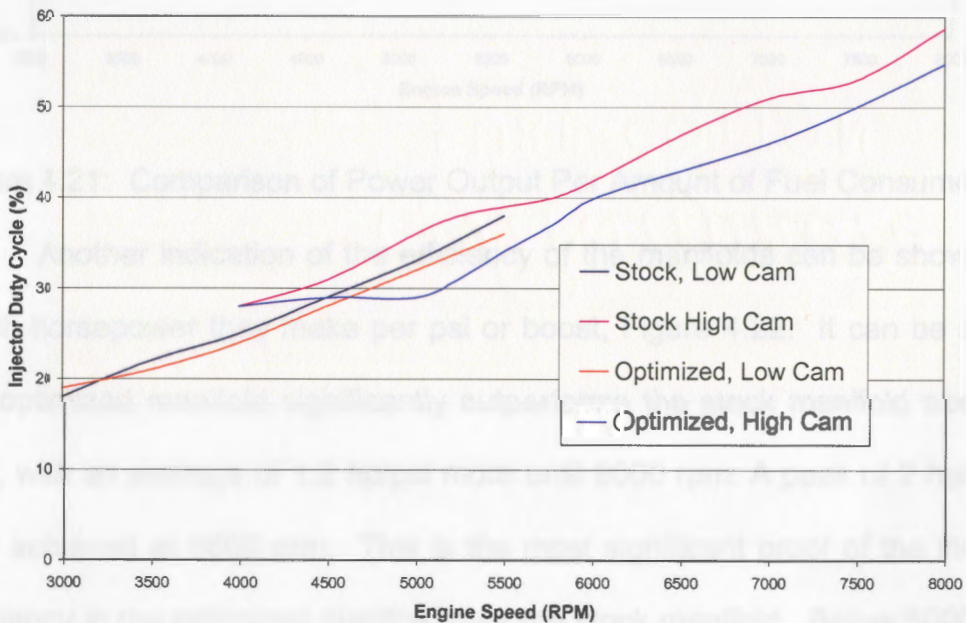


Figure 4.20: Fuel Injector Duty Cycle versus RPM for 11.5 psi Boost

The power output per unit of fuel consumption was also examined through the duty cycles of both systems, Figure 4.21. In this figure, it can be clearly seen that above 4500 rpm, the optimized manifold used less fuel to make the same power; yet another testament of the higher efficiency of the optimized manifold.

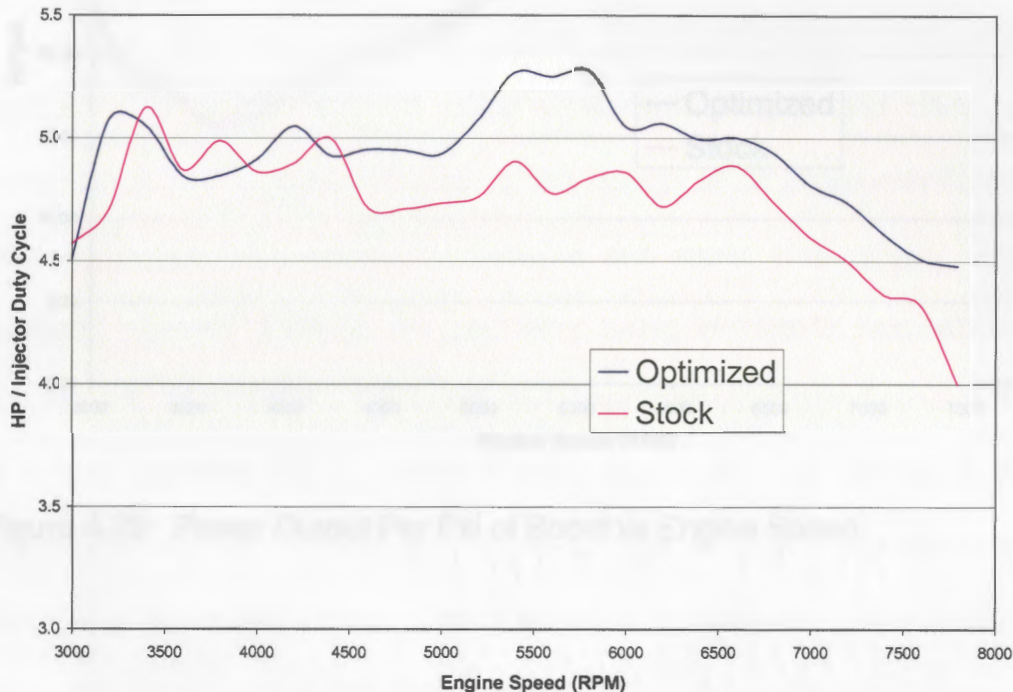


Figure 4.21: Comparison of Power Output Per Amount of Fuel Consumed

Another indication of the efficiency of the manifolds can be shown in how much horsepower they make per psi or boost, Figure 4.22. It can be seen that the optimized manifold significantly outperforms the stock manifold above 5000 rpm, with an average of 1.2 hp/psi more until 8000 rpm. A peak of 2 hp/psi more was achieved at 6800 rpm. This is the most significant proof of the increase in efficiency in the optimized manifold over the stock manifold. Below 5000 rpm the optimized manifold has an average of 0.5 hp/psi less.

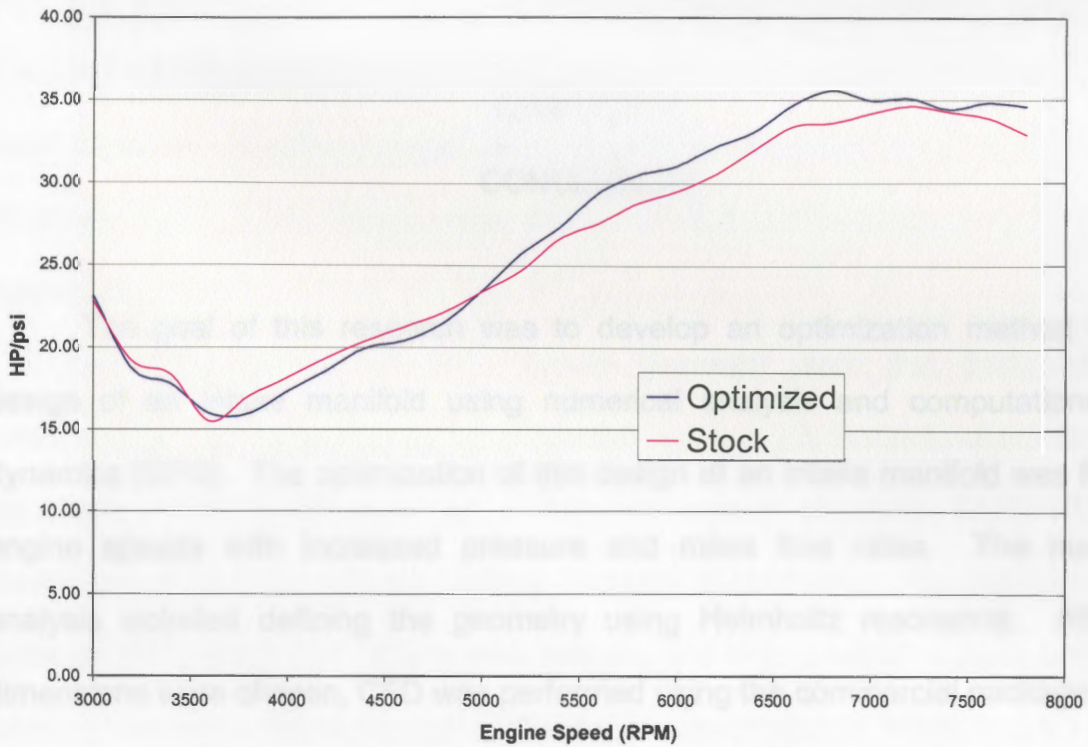


Figure 4.22: Power Output Per Psi of Boost vs Engine Speed

First the operating conditions were evaluated to correctly determine the boundary conditions at which the manifold would be optimized. The engine used in this research was a turbocharged modified 1637 cc dual-over-head-cam engine by Honda. Specifically the piston and was a B19A from an Acura (Honda's luxury division Integra LS, while the head was from an Integra GSR (B18C1) which employs Honda's variable valve timing and electronic lift control (VTEC). The VTEC allows the engine to effectively have two cam shafts: one optimized for low rpm and

CHAPTER V

CONCLUSION

The goal of this research was to develop an optimization method for the design of an intake manifold using numerical analysis and computational fluid dynamics (CFD). The optimization of this design of an intake manifold was for high engine speeds with increased pressure and mass flow rates. The numerical analysis included defining the geometry using Helmholtz resonance. After the dimensions were chosen, CFD was performed using the commercial package Fluent to further optimize the geometry of the runners and the plenum to ensure equal distribution of mass flow to all cylinders. The manifold was designed based on combining the results of the numerical and fluid analysis. The effectiveness of the new design was experimentally evaluated by comparing the torque curves, fuel consumption, and timing of stock and optimized manifolds.

First the operating conditions were evaluated to correctly determine the boundary conditions at which the manifold would be optimized. The engine used in this research was a turbocharged modified 1837 cc dual-over-head-cam engine by Honda. Specifically the bottom end was a B18A from an Acura (Honda's luxury division) Integra LS, while the head was from an Integra GSR (B18C1) which employs Honda's variable valve timing and electronic lift control (VTEC). This VTEC allows the engine to effectively have two cams shafts; one optimized for low rpm and

one for high rpm. The engine switches over to the high rpm cam based on a signal from the engine control unit (ECU). The engine was also turbocharged with a Garrett T3/T04B turbocharger and was often used for drag racing. Therefore, the most important operating conditions in this application were high rpm and under pressure from boost; these were the conditions for which the manifold was optimized.

As said, the runners and plenum geometry were first designed using Helmholtz tuning, analogous to a mechanical spring-mass system, where the tuned frequency is proportional to the gas velocity and system geometry, Section 3.1.2. A design speed of 6000 rpm was chosen because during racing the engine operates between 5000-8000 rpm. It was assumed that the engine will lack lower end power once optimized for the higher rpms. 6000 rpm was chosen in hopes that not all low-end torque would be sacrificed for street driving. Once the optimized RPM was chosen, the runner diameter, length and plenum size was manipulated to reach the chosen RPM.

The runner diameter of 2.25 inches was chosen because it would be easy to merge with the inlet port on the head, it minimized flow losses, and allowed sufficient spacing in the plenum. The plenum was simultaneously optimized in the commercial CFD package Fluent and yielded a volume of 248 in³. The inlet tract in the head was accounted for as well. Using the compression ratio of the engine as 10:1, and knowing the speed of sound in air, the manipulated Helmholtz equation, Equation 3.2, yielded a runner length of 7 inches.

The specific plenum shape was designed with the help of Fluent to monitor the mass flow rate during a revolution of the engine. A preliminary analysis was done in 2-D, Section 3.3, to test the boundary conditions. Once the methodology was perfected, it was then transferred to the 3D model. The boundary conditions were as such, the throttle body was a constant pressure mass-flow inlet and the outlets were either constant pressure outlets or walls. The outlet boundary conditions mimicked the opening and closing of the valves according to the cam duration, Table 3.1. Therefore 8 total boundary conditions were loaded with their own set of timesteps based on the cam duration, Figure 3.8.

A known problem in intake manifolds that are fed from one side and not from the center is that the end cylinder tends to receive the greatest amount of air. This is because the entering air wants to remain straight and goes to the end of the plenum where the number one cylinder is. Therefore the plenum was designed such that all cylinders would receive the same amount of air by tapering the plenum toward the number one cylinder. Nine variations, Table 3.2, of the slope of the back side of the plenum and runner height in the plenum were examined, Figure 3.10. The final dimensions are shown in Figure 5.1.

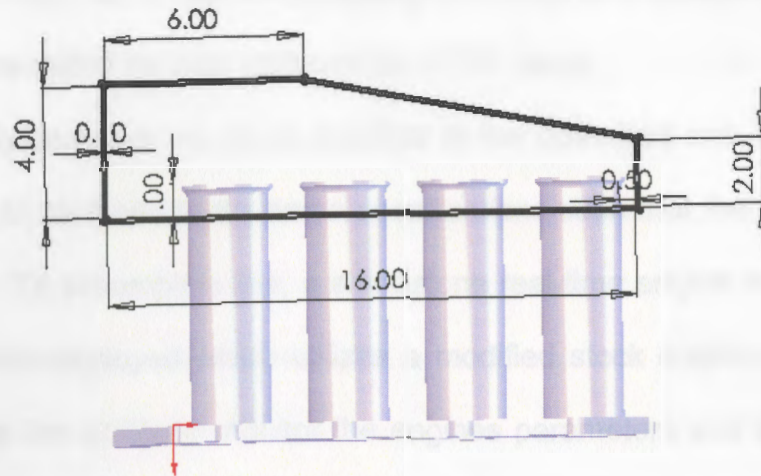


Figure 5.1: Final Dimensions of Plenum Shape

The optimized intake manifold was constructed completely out of mild steel. Flanges were made from $\frac{1}{2}$ in steel stock, the plenum from .049 in thick sheet metal, and the runners from .049 in thick piping. A transition 1 inch in horizontal length was made to accommodate a smoother transition for the throttle body to the plenum. The runners were welded into the base plate 1 inch from the top of the runner. The runner top was bellmouthed, Tallio et al, 1993, to $\frac{1}{4}$ in radius, Vorum, 1980, to make an effective entrance to the runner. The runners were then tapered to match the inlet port of the intake flange. Brackets and injector bosses were created to place the injectors and fuel rail in the stock position at the stock angle. 10 vacuum ports and the air intake temperature sensor were placed on the back of the plenum to ensure equal distribution to all vacuum operated devices. The idle air control valve was also removed from the intake manifold and mounted remotely. This was an advantage over the stock configuration because coolant runs through the idle air control valve and can heat up the intake manifold. One final advantage to the design of the

optimized manifold was that it has the possibility to accept all B-series VTEC heads because it has holes drilled for both styles of the VTEC head.

To effectively compare the stock manifold to the optimized one, both engine configurations had to be tuned to the same specifications such that the power could then be compared. To accomplish this, a standalone real-time engine management system, Crome, was employed which utilizes a modified stock engine control unit (ECU). Crome has the ability to monitor the engines parameters and the operator can make changes to the fuel and ignition tables accordingly. Both engines were tuned to an air/fuel ratio of 11.6-11.8 using an wideband oxygen sensor. Both setups were then run on a chassis dynamometer and the ignition was advanced until the engine stopped increasing in power. This is where the engine has reached its knock/predetonation limit and maximum power is being produced. Ideally, the dyno tests would have been run back-to-back on the same day, but this was not possible due to time constraints. The stock intake manifold was tested in about 55 degree weather with relatively low humidity and the optimized manifold was tested a week later in 70 degree weather during a rain storm with 100% humidity. The latter conditions are much poorer for making power. However, the conditions were close enough to make valuable comparisons.

The final fuel and ignition tables for both setups can be seen in Tables 4.1 – 4.8. The first testament to the greater efficiency of optimized manifold was that it required less timing to reach maximum power output. Over all, on the high cam the optimized manifold required about 3 degrees less timing than the stock manifold, while only requiring 1 more degree on the low cam, Figure 4.18. Since the injectors,

fuel rail, lines, fuel pressure riser, and fuel pump remained the same, a comparison about total fuel consumption could be made by examining the injector duty cycles. The optimized manifold required about 3 percent less fuel than the stock manifold at all boost levels on the high cam and about 1 percent less on the low cam, Figures 4.19 and 4.20. Figure 4.21 illustrates how the optimized manifold required less fuel to make more horsepower, showing that above 4500 rpm the optimized manifold outperformed the stock manifold. Below 4500rpm they were close to equal.

Comparing the horsepower per psi of boost is the clearest demonstration of the greater efficiency of the optimized manifold, Figure 4.22. The optimized manifold significantly outperforms the stock manifold above 5000 rpm, with an average of 1.2 hp/psi more until 8000 rpm and with a peak of 2 hp/psi at 6800 rpm. This is quite a meaningful difference. Below 5000 rpm the optimized manifold produced an average of 0.5 hp/psi less, which would be expected.

One final advantage to the optimized manifold was the decrease in air intake temperatures. Even though it was made out of a steel which has a lower coefficient of heat transfer than the stock aluminum, it was much thinner, therefore dissipating the heat much faster. After a short operation time, the stock intake manifold became heat soaked from the heat in the engine bay and was hot to the touch. The optimized manifold remained cool to the touch throughout all operation and under the same conditions lowered the air intake temperature by approximately 15-20 °F.

Overall, the optimized manifold was a much more efficient design for the given operating conditions and proved through experimentation the validity of the

methodology demonstrated in this research. With a little knowledge of an engine's operating conditions, this methodology could be applied to any configuration.

More testing, including a larger variety of loading conditions, in a closely controlled environment would yield more precise results with smaller deviations. It is the belief of this author that greater gains in power would be seen under higher loading conditions, such as higher rpms and greater airflow. There are some improvements that could be made in future revisions, but were not incorporated in this research due to manufacturing limitations that existed. These improvements include a longer, smoother taper into the head and being manufactured out of aluminum due to its higher coefficient of heat transfer.